Magnetic and Thermal Properties of $Tb(OH)_3$†

C. A. Catanese,* A. T. Skjeltorp, H. E. Meissner,‡ and W. P. Wolf
Yale University, Becton Center, New Haven, Connecticut 06520
(Received 13 March 1973)

Low-temperature measurements of magnetic susceptibility, magnetization, and specific heat have been made on single-crystal and polycrystal samples of $Tb(OH)_3$. The experimental techniques and methods of analysis were similar to those used previously to study isostructural $Gd(OH)_3$. The results are consistent with earlier reports that $Tb(OH)_3$ is a highly anisotropic ferromagnet resembling a three-dimensional Ising model, but a detailed analysis revealed an interesting range dependence of the effective spin-spin interactions. Estimates of the interactions between first-, second- and third-nearest neighbors were made from measurements at temperatures high and low compared with the Curie temperature ($T_C = 3.72 \pm 0.01$ K), using asymptotically exact series expansions correct to second order, and for both the first- and second-nearest neighbors an unusual cancellation between the magnetic dipole and "exchange" interactions was found. As a result of this cancellation, the net interaction between second-nearest neighbors becomes comparable to that between the nearest neighbors, but both are reduced in absolute magnitude so that they become comparable to the long-range dipole interactions between more distant neighbors. Some consequences of this competition on the cooperative properties are discussed.

I. INTRODUCTION

In a previous paper, [1] to be referred to as I, we outlined how measurements of susceptibility and magnetic specific heat could be combined with asymptotically exact calculations to give information about the interactions between the magnetic ions in the Heisenberg-like antiferromagnet $Gd(OH)_3$. We now report equally successful determination of the nondipolar interactions in the highly anisotropic isostructural ferromagnet $Tb(OH)_3$. [2]

Previous magnetic, [3] optical, [4,5] and thermal experiments[6] have shown that the low-temperature properties of the Tb^{3+} ions in this system can be described to a very good approximation as an Ising system, and preliminary estimates of the effective spin-spin interactions have recently been obtained. [7,8] In the present paper we shall refine these estimates and we shall examine in more detail the conditions which make $Tb(OH)_3$ one of the most interesting Ising-like systems known. [9,10] In particular it will be shown that each Tb^{3+} ion can be represented quite precisely by an effective spin $S' = \frac{1}{2}$, with effective spin-spin interactions of form $P'_{ij} S'_{zi} S'_{zj}$ and a Zeeman term given by $g_{\parallel}\mu_B S'_{zi} H_z$, where $g_{\parallel}$ is the g factor in the direction parallel to the hexagonal crystal c axis. Estimates of possible off-diagonal spin-spin and Zeeman interactions will show that all such terms should be quite negligible, so that the *form* of the Hamiltonian is very close to that of a simple Ising model. On the other hand, the interaction parameters P'_{ij} will turn out to have competing contributions from dipolar and nondipolar mechanisms, with the result that the *range* dependence will be quite different from the kind of nearest-neighbor Ising model usually studied.

The detailed analysis of the interactions is made possible by three special circumstances: First, the Ising-like form makes it possible to specify each pair interaction by a single parameter. Second, the hydroxide structure is such that all sites are magnetically equivalent, so that all pairs of a given type (e.g., nearest neighbor) can be described by one parameter. Third, the separation between nearest and next-nearest neighbors is significantly smaller than that of the third and more distant neighbors, so that we would expect only two significant nondipolar interactions. These considerations are the same as those invoked previously for the analysis of $Gd(OH)_3$ [1] except for the specific reason which limits each pair interaction to a single parameter. In the previous case this arose from the extreme *isotropy* of the S state of the Gd^{3+}, while in the present case it arises from the extreme *anisotropy* of the Tb^{3+} ions in the particular crystal field of the hydroxides. As before, we shall check the simplifying approximations by the internal consistency of the entire analysis.

In particular, we shall be able to show that the nondipolar contributions to the third- and more-distant-neighbor interactions must be quite small, so that these neighbors are only coupled by relatively weak magnetic dipole forces. However, as in the case of $Gd(OH)_3$, it will turn out that these weak interactions are really quite important for the cooperative properties, although for quite a different reason. In the $Gd(OH)_3$ case the second-nearest-neighbor interactions were found to be relatively strong, but their effect canceled to first order because of the particular *symmetry of the*

antiferromagnetically ordered state, and this enhanced the importance of the more-distant-neighbor interactions in the establishment of long-range order. In the present case, on the other hand, we shall find cancellations in the *contributions to the individual pair interactions* for both the nearest and next-nearest neighbors, which are thereby significantly weakened, and made comparable to the more-distant-neighbor interactions. Moreover, the effect of the long-range interactions in this system is enhanced, since $Tb(OH)_3$ orders ferromagnetically with long thin domains along the c axis for which the cumulative dipole sum is a maximum.

$Tb(OH)_3$ is thus of interest as a system which has the simple Ising *form* for the interactions but a range dependence which is more complicated than that of the usual near-neighbor models. In the present paper we shall be concerned mainly with the specification of the terms in the interaction Hamiltonian but we shall also present experimental data which may be of interest for comparison with subsequent calculations of the cooperative behavior.

In Sec. II we present a short description of structure of $Tb(OH)_3$ and the samples used, followed in Sec. III by a discussion of the Hamiltonian and a number of minor complications and corrections. Theoretical expressions relating the parameters in the microscopic Hamiltonian to measurable high- and low-temperature expansion coefficients of the susceptibility, magnetization, and specific heat are given in Sec. IV, and the experimental techniques are summarized briefly in Sec. V. The experimental results are described in Sec. VI and summarized in three tables (Tables III–V). The analysis to determine the effective spin-spin interaction parameters is given in Sec. VII, together with a brief discussion of some of the consequences of the unusual competitions which are found. The results are summarized in Table VI and the conclusions are discussed in Sec. VIII.

II. $Tb(OH)_3$ STRUCTURE AND SAMPLES

A. Structure

The hexagonal crystal structure of $Tb(OH)_3$ is identical to that of $Gd(OH)_3$ which has been described previously (see Sec. II A of I). The magnetic cation sublattice is shown in Fig. 1, which also gives several near-neighbor distances corresponding to $Tb(OH)_3$. The lattice constants used are $c = 3.57 \pm 0.01$ Å and $a = 6.28 \pm 0.01$ Å as reported by Klevtsov and Sheina.[11,12] These were also verified to within ± 0.01 Å from our own measurements.[13]

B. Samples

The $Tb(OH)_3$ single crystals and microscrystalline powder samples used in this work were prepared in this laboratory using a hydrothermal process, the details of which are given elsewhere.[13] The single crystals were generally about 1–10 mg in weight, in the form of hexagonal transparent prisms, parallel to the c axis (typically $10 \times 0.3 \times 0.3$ mm). Spectroscopic analysis confirmed negligible chemical impurities (< 0.1%), and x-ray diffraction checked for other phases, and in particular for the absence of the oxyhydroxide TbOOH in the microscrystalline samples (< 2%).

Altogether six different samples were used for the experiments reported in this paper and these are described in Table I. The table also includes the corresponding demagnetizing factors, whose definitions and uses were explained in I (Secs. II B and III B 1). Quite accurate estimates of the small demagnetizing factors for samples II and III could be obtained in the present case from measurements of the susceptibility in the ferromagnetic state, as described in Sec. IV G of this paper.

Samples I–IV were aligned by eye with an accuracy of about 3°. This corresponded to an uncertainty in the Curie constant of not more than ± 0.3%, and a possible error in higher-order terms in the susceptibility which was estimated to be quite negligible compared with other experimental errors. The alignment error in the measurement of the magnetization parallel to the c axis was similarly estimated to be small (< 0.2%) compared to other errors. For the measurement of the much smaller magnetization perpendicular to the c-axis alignment was more critical, but the appropriate orien-

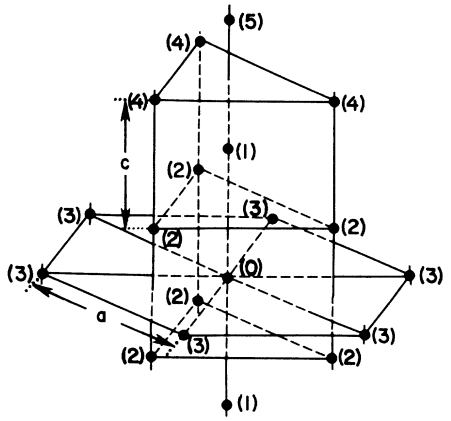

FIG. 1. Arrangement of Tb^{3+} ions in $Tb(OH)_3$. The successive neighbors and their distances (in Å) from the reference ion are as follows: (0) reference ion; (1) nearest neighbor ($1n$), 3.57 ($=c$); (2) next-nearest neighbor ($2n$), 4.04; (3) third nearest neighbor ($3n$), 6.28 ($=a$); (4) fourth nearest neighbor ($4n$), 6.47; (5) fifth nearest neighbor ($5n$), 7.14. One may note especially the relatively small distances between the nearest and next-nearest neighbors compared with the distance between the other neighbors.

tation could be found with negligible error ($< 0.2°$) by rotating the magnet after the sample was aligned approximately.

The powder samples used in the calorimetric measurements initially consisted of about 15-g powder mixed with about 6-g Apiezon N grease to improve thermal conductivity (sample V), but this introduced a significant uncertainty (about 3% at 10 K) due to the relatively large correction for the specific heat of the grease. In the later experiments a much larger powder sample (~ 70 g) was used (sample VI), and by careful mixing it was possible to reduce the amount of grease to less than 5 g while still preserving homogeneity and good heat contact. The larger sample also significantly reduced the relative importance of the corrections due to the thermometer, heater, and sample holder.

III. $Tb(OH)_3$ HAMILTONIAN

A. Effective-Spin Approximation

The low-lying levels of the Tb^{3+} ion in the hydroxide lattice have been studied by optical spectroscopy.[4,5] A crystal-field analysis showed that the ground state is actually two singlet states, the symmetric and antisymmetric combinations of nearly pure $|^7F_6, J_z = \pm 6\rangle$ with a small admixture of $|^7F_6, J_z = 0\rangle$, and in the absence of other interactions these are split by a small amount ($\epsilon_0 \simeq 0.4$ K).[14,15] The energy of the first-excited crystal-field state E_1 is about 170 K, and there is thus a wide range of conditions such that $\epsilon_0 \ll \mathcal{H}'$, $T \ll E_1$, where $\mathcal{H}'$ denotes the size[15] of other interactions (spin-spin, Zeeman, etc.). Under these conditions we can represent each Tb^{3+} ion by an effective spin $S' = \frac{1}{2}$, as is customary for systems with a well separated Kramers doublet ground state.[16] We shall show that this representation is in fact valid also for T comparable to or less than ϵ_0, provided $\mathcal{H}'$ remains much larger than ϵ_0. (See Sec. III C 4).

The linear Zeeman interaction can then be written as

$$\mathcal{H}_Z = \mu_B \vec{H} \cdot \overleftrightarrow{g} \cdot \vec{S}', \tag{1}$$

where the g tensor reflects crystal-field anisotropy and $\mu_B = |\mu_B|$ denotes the Bohr magneton. In the hexagonal symmetry of our present system, the g tensor is axially symmetric with two principal components, $g_\parallel$ along the hexagonal c axis and $g_\perp$ perpendicular to the c axis. Under the assumption of a pure $|J_z = \pm 6\rangle$ ground doublet, one obtains $g_\parallel = 18$ and $g_\perp \equiv 0$, and allowing for the small $|J_z = 0\rangle$ crystal-field admixture and the deviation from pure Russell-Saunders coupling one can find a more precise estimate[5] $g_\parallel = 17.87 \pm 0.05$ and $g_\perp = 0$. It should be noted that $g_\perp$ is zero to a very high degree of approximation and that the lowest-order splitting which will be produced by a field perpendicular to the c axis will arise from third-order effects proportional to H^3.

These predictions are in good accord with the experimental results. From the magnetic measurements discussed in this paper we estimate $g_\parallel = 18.0 \pm 0.2$ and $g_\perp < 1$ (see Sec. VI F), whereas optical measurements gave $g_\parallel = 17.7 \pm 0.2$. We shall therefore use the more accurate values estimated from the crystal-field analysis for all further calculations, and in particular for estimating the magnetic dipole-dipole interactions.

TABLE I. Summary of experiments and samples.

Sample no.	Type of measurements	Temperature region (K)	No. of single crystals	Total weight	Length (mm)/ Diameter (mm)	Demagnetizing factor $N_\parallel$[a]
I	High-field magnetization	1.1 – 4.2	1	0.8 mg	3/0.4	0.3 ± 0.1[b]
II	Low-field magnetization	1.1 – 4.2	1	1.0 mg	4/0.2	0.099 ± 0.010[c]
III	Low-frequency susceptibility	13.8 – 20	10	12.8 mg	7/0.6[d]	0.22 ± 0.01[c]
IV	High-frequency susceptibility	4.5 – 16	1	2.1 mg	16.5/0.3	0.015[b]
V	Specific heat	0.7 – 17	polycrystalline	15 g	...	...
VI	Specific heat	4 – 15	polycrystalline	70 g	...	...

[a] In units in which N for a sphere is $\frac{4}{3}\pi$.
[b] As estimated from ellipsoids of the same length to diameter ratio.
[c] As found from isothermal susceptibility measurements below T_C: $N_\parallel = 1/\chi_T$ with χ_T in emu/cm^3.
[d] Total diameter of the sample with the crystals laid side by side in a bundle.

B. Ising-Model Approximation

The extreme anisotropy of the g tensor immediately shows that the magnetic dipole-dipole coupling can be written

$$\mathcal{H}_{ij}^{\text{dip}} = D'_{ij} S'_{zi} S'_{zj} \quad , \tag{2}$$

with $D'_{ij} = g_{\parallel}^2 \mu_B^2 (r_{ij}^2 - 3z_{ij}^2)/r_{ij}^5$, where r_{ij} and z_{ij} denote relative positions of ions i and j. This has the desired Ising form and since $g_{\perp} \equiv 0$ there will be no other terms due to magnetic dipole-dipole coupling.

The form of the contribution of other interaction mechanisms is not so obvious. Any interaction which is bilinear in vector operators on the two sites will have a form in terms of the effective-spin operators similar to that of the magnetic dipole coupling and hence may be written

$$\mathcal{H}_{ij}^{\text{nondip}} = K'_{ij} S'_{zi} S'_{zj} \quad , \tag{3}$$

but the only physical mechanism known from first principles to be of this kind is isotropic exchange between the real spins ($J \vec{S}_i \cdot \vec{S}_j$). There is no reason to believe that this is the dominant nondipolar interaction in the present case.[9] More complicated mechanisms such as anisotropic exchange, electric multipole coupling, or virtual-phonon exchange can generally have matrix elements which are off diagonal between the two effective-spin states, and these could give rise to operators of the form $S'_{\pm i} S'_{\pm j}$.

Fortunately, however, such terms can be estimated to be very small in the present case. If we consider the most general form for an interaction between two magnetic ions characterized by angular momenta J_1 and J_2, we can always express it[9,17] phenomenologically by an operator of the form

$$\mathcal{H}' = \sum_{\substack{n,n' \\ m,m'}} J_{nn'}^{mm'} O_m^{(n)}(J_1) O_{m'}^{(n')}(J_2) \quad , \tag{4}$$

where the $O_m^{(n)}(J)$ are normalized spherical tensor (Racah) operators as defined by Smith and Thornley.[18] If such an operator acts on states which are built up from single electron states characterized by angular momenta l_1 and l_2, only terms with $n \leq 2l_1 + 1$ and $n' \leq 2l_2 + 1$ will have nonzero matrix elements[9,19] and this effectively truncates the expansion. In the present case the single electron states are well described by pure f states ($l_1 = l_2 = 3$) and this leads to $n, n' \leq 7$.

If we now consider an operator of this form acting on the particular doublet ground state which we have described by $S'_z = \pm \frac{1}{2}$, we see that off-diagonal terms will only occur to the extent that there is an admixture into the pure $|^7F_6, J_z = \pm 6\rangle$ states. This admixture can be estimated from the complete crystal-field analysis which shows that the amplitude of the $|^7F_6, J_z = 0\rangle$ component, α_0, is about 0.044, with all other admixtures identically zero or negligibly small. The only terms in Eq. (4) which can give off-diagonal matrix elements must therefore involve $m, m' = 0$ or ± 6.

For nearest neighbors there are additional restrictions due to the threefold axis of symmetry and horizontal reflection plane which result in the condition $m + m' = 0$. The only term which will have an off-diagonal matrix element will therefore be $J_{66}^{6-6} O_6^{(6)}(J_1) O_{-6}^{(6)}(J_2)$, and the order of magnitude of the corresponding matrix element will be $\alpha_0^2 J_{66}^{6-6} \sim 0.002 J_{66}^{6-6}$. If we make the reasonable assumption that the coefficient J_{66}^{6-6} will be comparable in magnitude to (or smaller than) the coefficient of the terms which result in diagonal matrix elements (e.g., J_{11}^{00}), we see that the off-diagonal terms will be less than 0.2% of the Ising terms for the nearest neighbors.

For next-nearest-neighbor pairs the symmetry is lower, and additional terms of the form $J_{66}^{60} O_6^{(6)}(J_1) O_0^{(6)}(J_2)$ will be allowed. These will have off-diagonal matrix elements of the order of $\alpha_0 J_{66}^{60} \sim 0.04 J_{66}^{60}$ which we may again estimate to be a small fraction of the Ising-like terms. Moreover, terms of this kind will appear in the effective-spin Hamiltonian as $S'_{\pm i} S'_{zj}$ which do not contribute to the energy of the ferromagnetic state in first order.

We can conclude, therefore, that the off-diagonal contributions from all sources will be extremely small, so that the effective spin-spin interaction can very precisely be described by the Ising form

$$\mathcal{H} = \sum_{i>j} P_{ij} \sigma_i \sigma_j + \tfrac{1}{2} g_{\parallel} \mu_B H \sum_i \sigma_i \quad , \tag{5}$$

where we have changed from $S'_{zi} = \pm \frac{1}{2}$ to $\sigma_i = \pm 1$ to conform to the usual Ising-model notation and we have also included the Zeeman term corresponding to an applied field along the c axis. The interaction parameters P_{ij} are given by

$$P_{ij} = K_{ij} + D_{ij} \tag{6}$$

with the dipolar interaction

$$D_{ij} = \tfrac{1}{4} g_{\parallel}^2 \mu_B^2 (r_{ij}^2 - 3z_{ij}^2)/r_{ij}^5 \quad . \tag{7}$$

We would expect that the nondipolar contributions K_{ij} would be significantly larger for nearest-neighbor and next-nearest-neighbor pairs, so that we can specify the complete interaction Hamiltonian by just two parameters K_1 and K_2, plus the magnetic dipole contribution calculated from the g value and lattice parameters [Eq. (7)].[20]

To check this assumption we shall include in the analysis a third adjustable parameter K_3 to represent possible nondipolar coupling between third-nearest neighbors, and we shall see that K_3 will in fact turn out to be very small, as we would expect. The over-all consistency of the analysis with only two adjustable parameters will also confirm that

there are no significant non-Ising terms which we have neglected, although it is hard to see where these could in fact come from. Even so, it is important to bear in mind that the theory of higher-order interactions is in such a poor state for predicting absolute magnitudes that our estimates of the non-Ising terms could well be off by quite a large factor.[21,22] It is comforting therefore that the extreme anisotropy of the Tb^{3+} ground state in the hydroxides eliminates the possibility of most contributions identically and reduces the remaining ones by very large factors. In other systems which are claimed to be Ising-like, such an extreme reduction is not always certain and the possibility of sizeable non-Ising terms always exists.

C. Minor Complications and Corrections

In addition to the electronic properties expressed in Eqs. (5)–(7), there are several minor complications which must be considered before theoretical expressions calculated using Eq. (5) can be related to the experimental results. The procedure outlined here is quite similar to a discussion for the Ising-like antiferromagnet dysprosium aluminum garnet (DAG), and we shall frequently refer to the analysis given for that system.[22]

1. Excited Electronic States

Some of the experiments reported later extended up to temperatures where effects from the excited states might not be negligible. The Schottky specific heat due to population of the excited state at E_1 was estimated as described in Ref. 22 (Sec. II C 1) and subtracted from all the calorimetric specific-heat measurements.[23] The maximum contribution was about 2% of the total specific heat at the highest temperature, 17 K.[24]

There is also a small contribution to the susceptibility due to the population of the first-excited state, but even at the highest temperatures of our measurements (25 K) the effect was less than 0.1% and thus completely negligible.

2. Van Vleck Paramagnetism and Diamagnetism

Some small contributions to the magnetic susceptibility result from a term in the Hamiltonian quadratic in the field. This arises from admixtures of excited electronic states[25] and there is also a small negative contribution due to diamagnetism which can be neglected here.[26] The only significant additional magnetic moment is due to the Van Vleck paramagnetism for a field H applied perpendicular to the hexagonal c axis,

$$m = \chi_{VV}^{\perp} H, \tag{8}$$

and using the crystal-field eigenfunctions determined spectroscopically,[5] one can estimate $\chi_{VV}^{\perp} = 5.9\times10^{-2}$ emu/mole. This compares favorably with the experimental value $\chi_{VV}^{\perp} = (6.8\pm1.1)\times10^{-2}$ emu/mole which we shall determine in (Sec. VI F). For field parallel to the c axis no significant Van Vleck contribution is predicted and none is found experimentally.[27]

3. Nuclear Effects

Naturally occurring terbium is isotopically pure 100% ^{159}Tb, which has nuclear spin $I = \frac{3}{2}$.[28] The corresponding hyperfine structure contributes to the total specific heat and magnetization, and these effects must be removed to isolate the intrinsic electronic properties. Although no detailed study of the hyperfine interactions has been made on $Tb(OH)_3$, we can use the experimental results from other Tb compounds following the procedure in Ref. 22 (Sec. II C 4). The spin Hamiltonian describing the hyperfine interaction for an ion in an axially symmetric crystalline electric field is given by[29]

$$\mathcal{H}_{hyp} = AS_z'I_z + B(S_x'I_x + S_y'I_y) + Q[I_z^2 - \tfrac{1}{3}I(I+1)] \ , \tag{9}$$

where the constants A and B are approximately proportional to the corresponding g values.[30,31] For $Tb(OH)_3$, $g_{\perp} \equiv 0$, and one can therefore neglect B. A can be determined from measured values of $A/g_{\parallel}$ for terbium ethyl sulfate,[28] and we get $A = 0.304$ K. An experimental value for the quadrupole constant Q is not available, but is expected to be small as found in related systems[28,32] and will be neglected here.

For a system which is Ising-like, the hyperfine contribution to the partition function can be calculated independently of the electronic interactions.[33] In particular, using the high-temperature expansion given by Bleaney[34] for the specific heat, one gets

$$(C/R)_{hyp} = S'(S'+1)I(I+1)A^2/9T^2 = b_{hyp}/T^2 \tag{10}$$

correct to order $1/T^4$, since one can easily show that term in $1/T^3$ is identically zero.[35]

Substituting values, this gives

$$(C/R)_{hyp} = (0.029\pm0.001)/T^2, \tag{11}$$

where the error limits include estimated uncertainties in the extrapolation procedure and the neglect of the quadrupole contribution.

As will be shown in Sec. VI B, this hyperfine specific heat starts to dominate the specific heat due to the electronic spins below about 1 K, and it would be satisfying to verify Eq. (11) experimentally. In Sec. IV D we will introduce an expression for the electronic contribution containing one parameter, and this, together with a possible hyperfine contribution of the form of Eq. (10), will be fitted to the experimental data. The result gives $b_{hyp} = 0.032\pm0.003$ K^2, in reasonable agreement with the calculated value [Eq. (11)].[36]

Using the same approximation to estimate nuclear effects on magnetic properties, one can readily show[33] that there is no contribution *to any order* from the $AS_z'I_z$ term, the only finite contribution coming from the usually neglected direct interaction of the nuclear moment with the applied field:

$$\mathcal{H}_{\text{nucl}} = g_n \mu_n \vec{I} \cdot \vec{H} \ . \tag{12}$$

However, this interaction is exceedingly small and its effect may be safely neglected at all but the lowest temperatures.

The simple separation of nuclear and electronic contributions to the thermodynamic properties is valid only for systems which are completely Ising-like, but this should be an excellent approximation for $Tb(OH)_3$ and we would therefore expect that any neglected cross terms would be extremely small.

4. Ground-State-Splitting Effects

Another effect which must be removed to isolate the intrinsic Ising-like properties of the electronic spin system is the contribution from the ground-state splitting ϵ_0 due to the crystal field (Sec. III A). The accurate computation of this effect for "high" ($T \gg T_C$) and "low" ($T \ll T_C$) temperatures is fairly simple as it may be accounted for by constructing an effective-spin Hamiltonian[28]

$$\mathcal{H}_{\text{cf}} = \epsilon_0 S_x' \ . \tag{13}$$

In particular, using the "high"-temperature expansion for the specific heat which is given in Sec. IV A 1, one gets

$$(C/R)_{\text{cf}} = \epsilon_0^2/4T^2 \simeq (0.04 \pm 0.01)/T^2 \tag{14}$$

correct to order $1/T^3$ (since the terms in $1/T^3$ are identically zero). This contribution corresponds to about 4% of the magnetic specific heat, and it can be allowed for with negligible uncertainty.

The "high"-temperature isothermal susceptibility χ_T will also contain a small effect due to the splitting given by[37]

$$(1/\chi)_{\text{cf}} \simeq \epsilon_0^2/12\lambda T \simeq (4.4 \pm 0.8) \times 10^{-4}/T \ (\text{emu/mole})^{-1}. \tag{15}$$

The effect from $\mathcal{H}_{\text{cf}}$ on the low-temperature properties of $Tb(OH)_3$ can be estimated in the limit of $T \to 0$. In this range the excitation spectrum of the crystal can be characterized by a single energy gap Δ_0 (see Sec. IV C), with $\Delta_0 = 9.0 \pm 0.2$ K. Additional terms of the form of Eq. (13) will have no first-order effect on this spectrum and the second-order shift will only be $\epsilon_0^2/2\Delta_0 \simeq 9 \times 10^{-3}$ K, which is negligible compared with other uncertainties in the present experiments.

At intermediate temperatures the effect of the small crystal-field effect is more difficult to assess. Intuitively, it would seem likely that an effect which is small at both high and low temperatures will also be small in the critical region. The problem is formally the same as that of an Ising model in a transverse magnetic field which has recently been discussed by Elliott *et al.*[38] who found strong indications that the critical behavior is relatively insensitive to a transverse field, and especially a very weak one. In particular, they concluded that the critical exponents may be *identically* the same as those of an Ising model in zero field, so that the only effect of the field would be to produce a small shift in the actual critical temperature. In any case, in the present study we are primarily concerned with the determination of the interactions and for this we can restrict our analysis to the two regions in which asymptotically exact estimates of the crystal-field effect can be made.

5. Phonon Effects

A detailed discussion of the lattice contribution C_L to the total specific heat C_T of several rare-earth hydroxides was given in I (Appendix B). An analysis similar to that used for $Gd(OH)_3$ gave an estimate of $C_L/R = (3.8 \pm 0.2) \times 10^{-5} T^3$ for $Tb(OH)_3$ in general agreement with direct calorimetric measurements[1] on diamagnetic $La(OH)_3$. At temperatures below 6 K this contribution amounted to less than 20% of the total with an uncertainty less than 1%, which was comparable to the error in the measurement of C_T. In this range estimates of $C_T - C_L$ thus provided a good measure of the magnetic specific heat C_M and an accurate check on the values obtained by the high-frequency method (see Sec. VI C). At higher temperatures the lattice contribution becomes rapidly dominant and much more reliable values of C_M can be obtained from the high-frequency method which is independent of C_L (see Sec. VI C).

IV. ASYMPTOTICALLY EXACT THEORIES

The method used to obtain values for the nondipolar interactions K_{ij} in our established form for the effective spin-spin Hamiltonian in Eq. (5) involves the use of "high"-temperature expansion for the susceptibility and "high"- and "low"-temperature expansions for the specific heat. An independent check is provided by the total internal energy and by a comparison with optical absorption measurements. The scale of high and low is set by the energies $k_B T$, K_{ij} ($\sim k_B T_C$), and $g_{\parallel}\mu_B H$, and the various expansions which we shall present are asymptotically exact for different temperature and field regions determined by T high and low compared with T_C and T high and low compared with $g_{\parallel}\mu_B H/k_B$. A quite detailed discussion along these lines has been presented for a similar Ising antiferromagnet in Ref. 22.

TABLE II. Dipolar and nondipolar interaction sums.

Single-center sums[a]	Double-center sums[b,c]	Triple-center sums[c,d]
$\Sigma_{rs}=\sum_j K_{ij}^r D_{ij}^s$ [e,f]	$\Delta_{21}=\sum_{j>k}(K_{ij}K_{jk}D_{ki})_p$	$\square_{31}=\sum_{j>k>l}(K_{ij}K_{jk}K_{kl}D_{li})_p$
	$\Delta_{12}=\sum_{j>k}(K_{ij}D_{jk}D_{ki})_p$	$\square_{22}=\sum_{j>k>l}(K_{ij}K_{jk}D_{kl}D_{li})_p$
	$\Delta_{03}=\sum_{j>k}D_{ij}D_{jk}D_{ki}$	$\square_{13}=\sum_{j>k>l}(K_{ij}D_{jk}D_{kl}D_{li})_p$
		$\square_{04}=\sum_{j>k>l}D_{ij}D_{jk}D_{kl}D_{li}$

[a] The sum $\sum_j$ is taken over all distinct pairs of ions i and j with ion i fixed as center and j running over all remaining ions.

[b] The sum $\sum_{j>k}$ is taken over all distinct triangles with ion i fixed as center and j and k running over all remaining ions.

[c] Subscript p denotes sums where a cyclic permutation of the coordinates is taken.

[d] The sum $\sum_{j>k>l}$ is taken over all distinct quadrangles with ion i fixed as center and j, k, and l running over all remaining ions.

[e] $D_{ij}=\frac{1}{4}g_n^2\mu_B^2(1-3z_{ij}^2/r_{ij}^2)/r_{ij}^3$.

[f] The shape dependence of the sum $\Sigma_{01}=\sum_j D_{ij}$ can be incorporated using a demagnetizing factor as discussed in Sec. IV A 2.

A. High-Temperature Zero-Field Specific Heat and Susceptibility

The high-temperature expansion in powers of $1/T$ for zero field is well known,[39–41] and only a summary of the calculations for our particular system is given in Secs. IV A 1 and IV A 2.[42]

1. Specific Heat

The magnetic specific heat per spin in zero field can be written as a high-temperature expansion of the form

$$\frac{C_M}{R}=\sum_{n=2}^{\infty}\frac{C_n}{T_n}=\frac{C_2}{T_2}+\frac{C_3}{T_3}+\cdots\ , \tag{16}$$

where C_2, C_3, ..., are related to sums of products of the interaction constants in the interaction Hamiltonian [Eq. (5)]. Specifically,

$$C_2=\frac{1}{2}\sum_j P_{ij}^2, \tag{17}$$

where the sum is taken over all distinct combinations of two ions with one ion i fixed as the center and j running over all the remaining ions. Similarly,

$$C_3=-2\sum_{j>k}P_{ij}P_{jk}P_{ki}, \tag{18}$$

where the sum is taken over all distinct combinations of three ions with one ion i fixed as the center and j and k running over all the remaining ions. Finally,

$$C_4=3\sum_{j>k>l}P_{ij}P_{jk}P_{kl}P_{li}-\frac{1}{2}\sum_j P_{ij}^4\ , \tag{19}$$

where the first sum is taken over all distinct combinations of four ions with one ion i fixed as the center and j, k, and l running over all the remaining ions. The last sum is defined as for C_2 in Eq. (17).

Expressing the P's in terms of the dipolar and nondipolar contributions [Eq. (6)] we find,

$$C_2=K_1^2+3K_2^2+3K_3^2+\tfrac{1}{2}\Sigma_{11}+\tfrac{1}{2}\Sigma_{02}, \tag{20}$$

$$C_3=-6(3K_1K_2^2+6K_2^2K_3+2K_3^3)-2\Delta_{21}-2\Delta_{12}-2\Delta_{03}, \tag{21}$$

$$C_4=3(12K_1^2K_2^2+12K_2^4+12K_3^4+72K_1K_2^2K_3+12K_1^2K_3^2+108K_2^2K_3+\square_{31}+\square_{22}+\square_{13}+\square_{04})-\tfrac{1}{2}(2K_1^4+6K_2^4+6K_3^4+4\Sigma_{31}+6\Sigma_{22}+4\Sigma_{13}+\Sigma_{04}), \tag{22}$$

where Σ_{nm}, Δ_{nm}, and $\square_{nm}$ are sums containing the dipolar interactions which are given explicitly in Table II. These sums are similar to corresponding expressions for $Gd(OH)_3$ and the technique used to evaluate them (using Yale IBM 7090–7094 and IBM 370/155) has already been explained in I (Appendix A). All the computer sums in C_2 and C_3 were checked indirectly against the corresponding sums for $Gd(OH)_3$ which in turn has been checked against published results for isostructural $GdCl_3$.[43] Substituting for the g value and lattice parameters given in Secs. II A and III A and evaluating the sums we finally obtain

$$C_2=K_1^2+3K_2^2+3K_3^2-(4.35\pm0.04)K_1+(1.864\pm0.019)K_2+(1.208\pm0.012)K_3+5.60\pm0.11, \tag{23}$$

$$C_3=-18K_1K_2^2-36K_2^2K_3-12K_3^3+(1.639\pm0.016)K_1^2-(4.25\pm0.04)K_1K_2+(30.8\pm0.3)K_2^2$$

$$-(2.54\pm0.03)K_1K_3-(33.1\pm0.3)K_2K_3-(9.07\pm0.09)K_3^2-(9.03\pm0.18)K_1$$
$$-(4.27\pm0.08)K_2-(8.56\pm0.17)K_3+7.4\pm0.2, \quad (24)$$

$$C_4=3[12K_1^2K_2^2+12K_2^4+12K_3^4+72K_1K_2^2K_3+12K_1^2K_3^2+108K_1^2K_3^2-(0.324\pm0.003)K_1^3+(14.09\pm0.14)K_2^3$$
$$+(14.84\pm0.15)K_3^3-(2.65\pm0.03)K_1^2K_2^2-(45.6\pm0.5)K_1K_2^2+(1.939\pm0.019)K_1^2K_3$$
$$-(42.8\pm0.4)K_1K_3^2+(52.2\pm0.5)K_1K_2K_3-(89.3\pm0.9)K_2^2K_3+(112.1\pm1.1)K_2K_3^2$$
$$+(1.84\pm0.13)K_1^2+(79\pm2)K_2^2+(83\pm3)K_3^2+(31.6\pm0.9)K_1K_2+(6.7\pm0.6)K_1K_3$$
$$+(13.8\pm1.3)K_2K_3+(2.42\pm0.17)K_1-(23.6\pm1.2)K_2+(1250\pm60)K_3-(2.23\pm0.15)]$$
$$-\tfrac{1}{2}[2K_1^4+6K_2^4+6K_3^4-(17.49\pm0.18)K_1^3+(7.50\pm0.08)K_2^3+(4.82\pm6.05)K_3^3$$
$$+(57.34\pm0.12)K_1^2+(3.52\pm0.07)K_2^2+(1.45\pm0.03)K_3^2-(83.6\pm2.5)K_1$$
$$+(0.73\pm0.02)K_2+(0.194\pm0.006)K_3+45.8\pm1.8], \quad (25)$$

where we have included in C_2 the small crystal-field and hyperfine contributions which accounts for only about 7% of the total (Secs. III C 3 and III C 4). The error limits are the over-all accuracy estimated from the g value, lattice constants, and determination of the sums themselves. These expressions will be combined in Sec. VII with a similar expansion for the susceptibility to yield values for the three non-dipolar interaction parameters K_1, K_2, and K_3.

2. *Susceptibility*

The high-temperature expansion for the parallel isothermal susceptibility in zero field is most conveniently written as[44]

$$\chi_T(0)=\lambda/(T-\theta+B_2/T+B_3/T^2+\cdots). \quad (26)$$

Here λ is the Curie constant, and if $\chi_T(0)$ is expressed in emu/mole, we calculate $\lambda=N_0g_{\parallel}^2\mu_B^2/4k_B=29.95\pm0.17$ emu K/mole using $g_{\parallel}=17.87\pm0.05$ (Sec. III A). We will occasionally also express $\chi_T(0)$ in emu/cm^3 with the corresponding Curie constant $\lambda_v=\lambda/V_0$, where V_0 is the gram atomic volume. V_0 can be calculated from the lattice constants given in Sec. II A which give $V_0=36.7\pm0.4$ cm^3 and therefore $\lambda_v=0.816\pm0.010$ (emu K/cm^3).

The first three coefficients which depend on the interactions in Eq. (26) are

$$\theta=-\sum_j P_{ij}, \quad (27)$$

$$B_2=\sum_j P_{ij}^2, \quad (28)$$

$$B_3=-2\sum_{j>k}P_{ij}P_{jk}P_{ki}+\frac{2}{3}\sum_j P_{ij}^3, \quad (29)$$

with the summation convention as defined in Sec. IV A 1. Comparing Eqs. (28) and (17) we see that

$$B_2=2C_2, \quad (30)$$

which will later prove to be a useful check of our analysis of the experimental results.

Furthermore, comparing Eqs. (29) and (18), we see that

$$B_3=C_3+\frac{2}{3}\sum_j P_{ij}^3. \quad (31)$$

It is important to note carefully the definition of the parameter θ in Eqs. (26) and (27) which is here the first term in an *exact* high-temperature expansion, in contrast to the more usual "Curie-Weiss θ" which is used to fit experimental data in the molecular-field approximation. As $T\to\infty$, the two θ's become the same, but the more precise definition of θ given in Eq. (27) makes it possible to relate this quantity to other parameters without any uncertainties due to statistical approximations.

Expressing the P's in terms of dipolar and non-dipolar contributions, we find

$$\theta=-2(K_1+3K_2+3K_3)-\Sigma_{01} \quad (32)$$

and

$$B_3=C_3+\tfrac{4}{3}(K_1^3+3K_2^3+3K_3^3)+\tfrac{2}{3}(3\Sigma_{21}+3\Sigma_{12}+\Sigma_{03}), \quad (33)$$

where the dipolar sums Σ_{pq} are again given in Table II. In contrast to the other dipole sums, Σ_{01} in θ is shape dependent and it was convenient to calculate it for all ions within a series of spheres of increasing radii (up to 100 Å), and estimating the limiting value as $R\to\infty$. The shape dependence could be incorporated using a demagnetizing factor $N_{\parallel}$ as discussed in I [Eq. (5a)]. Substituting for the dipole interactions, the final values for θ and B_3 were thus found to be

$$\theta=-(K_1+3K_2+3K_3)+(2.26\pm0.02)-(N_{\parallel}-\tfrac{4}{3}\pi)\lambda_v, \quad (34)$$

where $\lambda_v=0.816$ (emu K/cm^3), as given above, and

$$B_3=C_3+\tfrac{4}{3}(K_1^3+3K_2^3+3K_3^3)-(8.74\pm0.09)K_1^2+(3.75\pm0.04)K_2^2+(2.41\pm0.02)K_3^2+(19.1\pm0.4)K_1$$
$$+(1.17\pm0.02)K_2+(0.48\pm0.01)K_3-13.8\pm0.4, \quad (35)$$

where the error limits are determined as for the specific-heat coefficients in Sec. IV A 1.

For the comparison of different experimental results we shall correct all θ values to a common shape which in the present case is most conveniently chosen to be an infinitely long and thin shape with $N_{\parallel}=0$. The corresponding value will be denoted by θ^{∞}.

B. High-Temperature and Low-Magnetic-Field Magnetization

In connection with the high-frequency specific-heat measurements (Sec. V D), we will need an approximation for the magnetization $M(H, T)$ as a function of field and temperature for $g_{\parallel}\mu_B H/k_B \ll T$ and $T \gg T_C$. As explained in I, an adequate approximation for M can be written under these conditions in the convenient form[45]

$$M=\frac{\lambda H}{T-\theta+B_2/T+B_3/T^2}-\frac{\lambda^2 T H^3}{3R(T-\theta+7B_2/4T)^4} \quad (36)$$

which corresponds to the leading terms of a more complete expression obtained previously.[22] Here $R=N_0 k_B$ denotes the molar gas constant and the other symbols are the same as those used in the low-field expression [Eqs. (26)–(29)].

C. Low-Temperature Specific Heat

In an Ising system, excitations of the fully ordered state ($T\to 0$) take the form of localized spin flips.[46] These excitations may therefore be accurately described in terms of a simple energy gap Δ_0 and there is corresponding low-temperature specific heat of the form

$$\frac{C}{R}=\left(\frac{\Delta_0}{T}\right)^2\frac{e^{\Delta_0/T}}{(1+e^{\Delta_0/T})^2} \quad (37)$$

Not surprisingly, this has the same form as the low-temperature tail of a Schottky specific-heat anomaly of a two-level system, but in contrast to the latter it is strictly valid only in the limit $T/\Delta_0 \to 0$. At higher temperatures multiple spin flips become important and a more complex expression must be used. The method of extracting Δ_0 from measurements of finite temperatures has been outlined in Ref. 22 and we shall discuss it further in Sec. VI B.

The energy gap of an Ising system can also be obtained from an estimate of the internal energy in the fully ordered state, which can be obtained by integrating the specific heat[22] (see Sec. VI D). If we denote the energy per spin at $T=0$ K by U_0/R and choose the energy of the fully disordered state as zero, we can readily show that

$$-U_0/R=\tfrac{1}{4}\Delta_0 \ . \quad (38)$$

The energy can also be related to the interactions defined in Eq. (5):

$$-\frac{U_0}{R}=\frac{1}{2}\sum_j P_{ij} \ , \quad (39)$$

and comparing Eqs. (27), (28), and (39) we see that

$$\Delta_0=2\theta^{\infty}, \quad (40)$$

where we have chosen the value of θ appropriate to zero demagnetizing factor to reflect the fact that the ordered state will take the form of domains which minimize the magnetostatic energy. Strictly speaking, we should also allow for additional contributions to the total energy from domain walls and residual magnetostatic surface energies, but rough estimates show that these effects will be negligible in the present case.

The three equations (38)–(40) provide convenient cross checks of both the experimental results and the method of analysis and we shall see later (Sec. VI H) that very satisfactory consistency is in fact obtained.

D. Low-Temperature High-Field Magnetization

The low-temperature magnetization for an Ising system has been discussed in Ref. 22, where it was shown that

$$M=M_0\tanh\left[(g_{\parallel}\mu_B H/k_B+\Delta_0)/2T\right] \quad (41)$$

with $M_0=\frac{1}{2}N_0\mu_B g_{\parallel}$. In the case of $g_{\parallel}\mu_B H/k_B \gg \Delta_0$ this expression reduces to the simple expression for the Brillouin function for $S'=\frac{1}{2}$, and for $Tb(OH)_3$ this simplification holds to within 0.3% for $H>7$ kG and $T<2.5$ K. It is therefore possible to obtain a value for M_0, and hence the g value, by measuring M at high fields, and taking the asymptotic value for $M/\tanh(g_{\parallel}\mu_B H/2k_B T)$. In a general case one should also consider the temperature-independent contribution to M, but for $Tb(OH)_3$ this was shown earlier to be negligible (Sec. III C 2).

V. EXPERIMENTAL METHODS

The apparatus and experimental methods were essentially the same as those used previously for the study of $Gd(OH)_3$, and details may be found in I and also in Refs. 47–50. We shall therefore summarize here only those details which are peculiar to our present study of $Tb(OH)_3$.

A. Specific-Heat Measurements

Two different techniques were used to estimate the magnetic specific heat C_M. One was to use the standard electrical heat-pulse method[47] to determine the total specific heat C_T and to allow for a lattice contribution C_L estimated from an analysis of the high-temperature variation of $C_T=C_M+C_L$. In the present case C_L could only be estimated with an uncertainty of about 5% (see I, Appendix A), and it was therefore possible to deduce C_M only in regions where the lattice correction was not too

large. This condition was well satisfied below about 5 K where C_L was less than 3% of C_M, but at higher temperatures the ratio between C_L and C_M increased rapidly (roughly as T^5). Thus, at 12 K C_L accounted for 90% of the total, resulting in a 50% uncertainty in C_M. For our quantitative analysis we therefore used the calorimetric measurements only below about 10 K. In this range the uncertainty due to the corrections for the calorimeter and the grease used to promote thermal contact was also small (see Sec. II B), and we estimate an over-all accuracy in our final values of C_M from 2 to 20% in the temperature range 4–10 K.

To measure C_M at higher temperatures we used the high-frequency method of Casimir and du Pré.[48,49,51,52] In this one measures the field dependence of the adiabatic magnetic susceptibility $\chi_S(H)$, which is directly related to C_M by a thermodynamic expression involving only derivatives of M with respect to T and H. In the present case, these derivatives could be estimated with adequate accuracy from the theoretical expression given in Eq. (36) and the main problem revolved around measuring $\chi_S(H)$. In particular, it was necessary to establish at the outset the conditions under which the measuring frequency f would satisfy the condition

$$1/\tau_{SL} \ll 2\pi f \ll 1/\tau_{SS}, \tag{42}$$

where τ_{SL} and τ_{SS} are the spin-lattice and spin-spin relaxation times.

The first of these inequalities, $1/\tau_{SL} \ll 2\pi f$, can generally be assured by varying the temperature, since τ_{SL} is always a strong function of temperature, becoming quite long (~ msec) at helium temperatures. This was confirmed in the present case by rough theoretical estimates based on the approximations given by Orbach,[53] using available crystal-field parameters. Details of the calculation are given elsewhere,[54] but the results showed clearly that τ_{SL} should be longer than about 9×10^{-3} sec at 5 K, with a dominant Raman process varying approximately as $\tau_{SL} \sim 700T^{-7}$ sec. For experimentally convenient frequencies in the range 2–4 MHz, this corresponds to a maximum temperature of about 30 K below which Eq. (42) should be well satisfied. This was confirmed by the final measurements of C_M which gave a smooth variation up to about 20 K, where there was an abrupt kink which we interpret as the breakdown of the first inequality in Eq. (42).[55]

The second inequality, $1/\tau_{SS} \gg 2\pi f$, is more difficult to test. The general order of magnitude of spin-spin relaxation times is 10^{-10}–10^{-12} sec, essentially independent of temperature, and we might therefore expect that a measuring frequency in the range 2–4 MHz would easily satisfy Eq. (42). However, in an extremely anisotropic system such as $Tb(OH)_3$ the "flip-flop" terms which are generally responsible for spin-spin relaxation[56] are very small (see Sec. III B), and we must therefore expect significantly longer times for τ_{SS}. Under these conditions it is very difficult to estimate τ_{SS} theoretically, but we can fortunately test for the inequality in Eq. (42) empirically in two different ways.

One is to compare values of the zero-field susceptibility as estimated from the measured frequency shifts and the filling factor of the rf coil with values measured at lower frequencies (Sec. VI E) or calculated theoretically.[48,49] Agreement between these estimates indicates that the spins come into internal equilibrium in times short compared to the measuring rate, as required by the relaxation condition [Eq. (42)]. In the present experiments, such agreement was in fact found to within the estimated uncertainty of the calculated filling factor (~ 20%).

An independent confirmation of Eq. (42) was provided by the agreement of the observed field dependence of the rf susceptibility with that predicted by the Casimir-du Pré theory,[49,51,52] and also by the quantitative agreement between the inferred values of C_M and those estimated from the total specific heat. This test should be quite sensitive, since τ_{SS} is generally a strong function of field,[56] and if spin-spin relaxation were affecting the susceptibility measurements, one would expect a marked effect in the observed field dependence.[49,57]

We may conclude from all this that measuring frequencies in the range 2–4 MHz do satisfy both relaxation conditions specified in Eq. (42) for all temperatures below 20 K, so that measurements of the real part of the susceptibility $\chi'(H)$ should correspond to the thermodynamically defined adiabatic susceptibility $\chi_S(H)$.[58]

The magnetic specific heat per spin is then related to the field dependence of $\chi'(H)$ by[49,51,52,58]

$$\frac{C_M(H,T)}{R} = \left[T\left(\frac{\partial M}{\partial T}\right)_H^2 \Big/ R\chi_T(H)\right]\left(\frac{\chi'(0)\chi_T(H)}{\chi'(H)\chi_T(0)} - 1\right)^{-1}, \tag{43}$$

where $\chi_T(0)$ and $\chi_T(H)$ denote the isothermal susceptibilities $(\partial M/\partial H)_{T,H=0}$ and $(\partial M/\partial H)_{T,H}$, respectively. Using the expression for M given in Eq. (36) which is adequate for the range of H and T of the present measurements, we find

$$\frac{C_M(H,T)T^2}{R} \approx \frac{\lambda}{R}\left(\frac{T}{T-\theta+B_2/T+B_3/T^2}\right)^3\left(1-\frac{B_2}{T}-\frac{2B_3}{T^2}\right)^2 \times r(H,T)\left(1+\frac{\lambda}{R}r(H,T)\frac{T(T-\theta+B_2/T)}{(T-\theta+7B_2/4T)^4}\right), \tag{44}$$

where

$$r(H, T) = H^2\left[\frac{\chi'(0)}{\chi'(H)} - 1\right]^{-1} \tag{45}$$

and the other parameters have been defined in Eqs. (26) and (36). Values of the parameters λ, θ, B_2, and B_3 were estimated experimentally as discussed in Sec. VI E, and the values used in the final analysis are listed in Table IV.

As discussed in I, $C_M(H, T)$ is generally field dependent and it is convenient to extract the zero-field value $C_M(0, T)$ which is most directly related to the spin-spin interactions [Eq. (16)]. For this we could in principle extrapolate measurements in "large" fields, but it was here more convenient to limit the measuring fields so that the field dependence was practically negligible. To estimate the field dependence we used the theoretical relation given in I (Sec. IV A) together with Eq. (36):

$$\frac{C_M(0, T)T^2}{R} = \frac{C_M(H, T)T^2}{R} + \frac{(B_2 + 3B_3/T)(\lambda/R)H^2}{(T - \theta + B_2/T + B_3/T^2)^2}\ , \tag{46}$$

which is correct to second order in H. In the present experiments it was possible to limit H so that the last term in Eq. (46) was always less than 0.2% of first term, so that the field dependence was in fact negligible.[59] From Eq. (44) we see that $r(H, T)$ is then only a function of T, $r(T)$, which could thus be determined simply from plots of $\chi'(0)/\chi'(H)$ vs H^2.

At the lowest temperatures ($T < 5$ K) it is possible that our simplified treatment is no longer adequate and that higher-order terms in H and the interactions should be included. However, in this range the total specific-heat measurement provided an entirely satisfactory estimate of C_M, and a direct comparison of both methods over the region of overlap 4.5–10 K gave very satisfactory agreement, as will be seen in Sec. VI C.

B. Isothermal Susceptibility Measurements

Susceptibility measurements were performed at liquid-hydrogen temperatures (13.9–20.0 K) using audio-frequency inductance method of McKim and Wolf[50] (see also I, Sec. IV B). The limit of detection of the apparatus was 10^{-7} emu, corresponding to a relative accuracy of ± 0.1%, in the temperature dependence of $\chi_T(0)$ for the particular sample (III) which was used (see Table I). The temperature was determined from the vapor pressure above the liquid with an estimated accuracy of about ± 0.01 K, so that the over-all accuracy of the $\chi_T(0)$ vs T variation was better than ± 0.2%. The absolute accuracy, which also involves the calibration of the apparatus and the weight of the sample, was estimated to be about ± 1%.

Additional estimates of the isothermal susceptibility were obtained from the high-frequency measurements in zero applied field. As discussed in Sec. V A there was strong evidence that spin-spin relaxation was faster than the measuring frequencies of 2–4 MHz, and under this condition the zero-field susceptibility is equal to the isothermal susceptibility, even though, as in our case, the spin-lattice relaxation may be much slower. This is simply because $\chi_S(H) \to \chi_T(H)$ as $H \to 0$.

Details of the apparatus and the methods for allowing for the dielectric contribution to the measured frequency shifts have been given elsewhere.[48,49] For the small single crystals used in the present experiments it was difficult to obtain an accurate estimate of the effective filling factor of the rf coil (better than 20%), and only relative measurements of the susceptibility were therefore made. However, these could readily be normalized (to within 1%) by comparing them with the low-frequency measurements made in the other apparatus. Since the high-frequency apparatus incorporated an independent temperature-control system, it was thus possible to extend the isothermal susceptibility measurements outside the liquid-hydrogen range covered by the low-frequency apparatus. The accuracy of the temperature measurements in this system was estimated to be about ± 0.01–0.08 K over the range 4.5–25 K, respectively, and the relative accuracy of the susceptibility measurements was about ± 3%. No measurements were made at higher temperatures because of contributions to the susceptibility due to the population of the first-excited state (Sec. III C 1).

C. High-Field Magnetization Measurements

Measurements of the magnetic moment parallel to the c axis were carried out in fields up to 14 kOe at temperatures between 1.1 and 4.2 K using a vibrating-sample magnetometer[60] as described elsewhere.[47] The limit of detection was about 2×10^{-4} emu, corresponding to about 0.1% of the saturation moment of our $Tb(OH)_3$ sample. However, the absolute accuracy which depends on calibration was again lower, and it was estimated to be about ± 1%.

Measurements were also made with the field perpendicular to the c axis, and for these a very small moment ($\sim \frac{1}{50}$ of the parallel moment) was found. As a result of this, very careful alignment of the magnetic field was required and this was achieved by rotating the magnet, as discussed previously (Sec. II B). With proper adjustment (± 0.2°) no significant additional error in $M_\perp$ was incurred. However, the much smaller values of $M_\perp$ resulted in less accurate measurements, and the typical scatter was about ± 10%. No attempt was made to study the angular dependence of $M_\perp$ in the plane perpendicular to the c axis since the anisotropy would be expected to be extremely small.

D. Low-Field Magnetization Measurements

To study the low-field temperature dependence of the magnetization, especially in the vicinity of the critical point ($T_c = 3.7$ K) additional measurements were made using a ballistic method. The apparatus was essentially the same as that used for the ac susceptibility measurements,[50] using a moving sample and a compensated pair of pickup coils inside the Dewar. Static magnetic fields up to 900 Oe were provided by an external solenoid. The voltage pulse resulting from the motion of the magnetized sample from one secondary to the other was measured either with a ballistic galvanometer (Tinsley 4789) or with an integrating digital voltmeter (Dymec 2401 C). The former was more sensitive ($\pm 6\times10^{-5}$ emu)[61] and was used for small moments (up to 0.05 emu), while the latter had a sensitivity of only $\pm 5\times10^{-4}$ emu[61] but was much more convenient for measuring larger moments.

Calibration of both measuring systems was carried out using manganous ammonium sulphate,[50] and the estimated absolute accuracy was about $\pm 0.5\%$. Temperatures were measured from the vapor pressure of liquid helium outside the sample space, which was filled with low-pressure helium gas for thermal contact. The estimated accuracy of the temperature measurements in the region 1.2–4.2 K varied from about 0.02 to 0.005 K, respectively.

VI. EXPERIMENTAL RESULTS

A. Analysis in Terms of Characteristic Parameters

In this section we shall present various experimental results in such a way that we can readily extract the different characteristic parameters which describe the magnetic and thermal properties of $Tb(OH)_3$. These parameters are of three kinds[22]: (i) single-ion parameters which characterize the interactions of individual Tb^{3+} ions with their immediate environment, (ii) collective parameters which describe the effect of spin-spin interactions in regions well removed from cooperative phase transitions, and (iii) critical parameters which characterize the phase transitions themselves.

In the present work we have concentrated mainly on (i) and (ii), since these can be studied more easily with available samples, but one would hope that subsequent experiments will give equally detailed information on the cooperative properties and a comparison with the predictions of the appropriate Ising model. Some of the difficulties of making critical-point measurements on $Tb(OH)_3$ will be reviewed in Sec. VI G, but we shall first extract four single-ion parameters (M_0, λ, $\chi^{\perp}_{\nu\nu}$, and b_{hyp}) and eight collective parameters (θ^{∞}, B_2, B_3, C_2, C_3, C_4, Δ_0, and U_0) using the theoretical expressions given in Sec. IV. Several of these parameters can be related to one another, providing tests of both the theoretical approximations and the experimental technique. The results of all the parameters will be summarized in Sec. VI H and a final set of four basic independent parameters θ^{∞}, C_2, C_3, and C_4 will be established. This set will then be used in Sec. VII for the determination of the nondipolar interactions.

B. Magnetic Specific Heat from Calorimetric Measurements

The results of the total specific-heat measurements corrected for the calorimeter and grease contributions are shown as the filled circles in Fig. 2. The corresponding magnetic specific heat was estimated by subtracting a lattice contribution determined from the usual plot of $C_T T^2/R$ vs T^5 which gave $C_L/R = (3.8\pm0.2)\times10^{-5}T^3$. Some of the uncertainties inherent in this procedure were discussed in I (Appendix B), and the present error limit is based on a comparison with the range of results obtained for some of the other hydroxides. The corresponding uncertainty in the estimated magnetic specific heat becomes relatively small below about 7 K, but at higher temperatures the error on C_M increases rapidly. The estimates of C_M in this range were therefore only used to check on the consistency of the high-frequency measurements, as discussed in Sec. VI C.

The low-temperature results showed a fairly

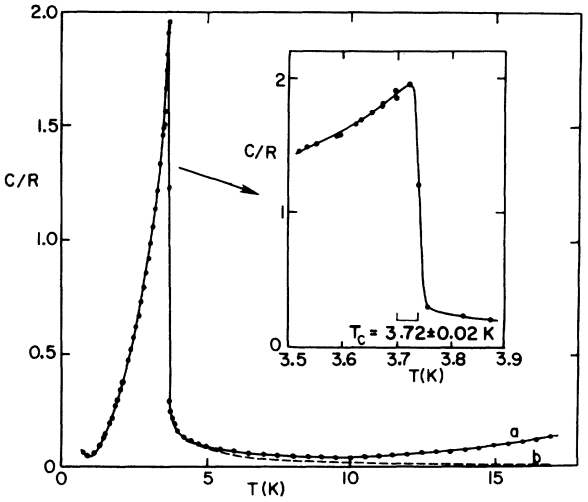

FIG. 2. Specific heat of $Tb(OH)_3$ from calorimetric measurements. Closed circles (curve *a*), total specific heat C_T/R, as measured. Broken line (curve *b*), magnetic specific heat C_M/R obtained by subtracting an estimated lattice contribution $C_L/R = 3.8\times10^{-5}T^3$. The temperature of the λ peak was estimated at $T_C = 3.72 \pm 0.02$ K (see expanded scale insert). The rise in the specific heat with decreasing temperature for $T < 1$ K is due to hyperfine interactions.

sharp peak at 3.72 ± 0.02 K which we shall interpret as the ferromagnetic Curie point T_C (see Sec. VI G). A more detailed study of the peak revealed a significant amount of "rounding" (~ 0.02 K) which is of course not surprising in view of the polycrystalline nature of the present samples. No attempt was therefore made to investigate the shape of the specific-heat curve in the vicinity of T_C.

At even lower temperatures a rounded minimum was observed, and this may readily be explained by the sum of a hyperfine contribution [Eq. (11)] and a spin-spin contribution of the form of Eq. (37). To obtain the best experimental values for b_{hyp} and Δ_0 the raw data were fitted to an expression of the form

$$\frac{C_M}{R} = \frac{b_{hyp}}{T^2} + \left(\frac{\Delta_0}{kT}\right)^2 \frac{e^{\Delta_0/kT}}{(1+e^{\Delta_0/kT})^2} \tag{47}$$

using a computer least-squares fitting program, for several choices of the number of experimental points to be fitted. Since a spin-spin term of the form of Eq. (47) is valid only in the limit of $T/\Delta_0 \to 0$ we would expect a small systematic variation in the effective value of Δ_0 as fewer higher-temperature points are included in the fit, and by extrapolating the results to $T = 0$ K one can thus estimate the true gap parameter Δ_0. This procedure was discussed in some detail in Ref. 22. The results of this analysis gave

$$b_{hyp} = 0.032 \pm 0.003 \text{ K}^2 \tag{48}$$

and

$$\Delta_0 = 8.5 \pm 0.5 \text{ K}, \tag{49}$$

where the errors reflect uncertainties due to the approximations in the analysis as well as experimental errors. The value of b_{hyp} is in quite good agreement with the calculated value [Eq. (11)] and the estimate of Δ_0 is in fair agreement with previous optical determinations[5] and also with other estimates to be discussed later in this section.

C. High-Frequency Specific-Heat Measurements

Measurements of the field dependence of the adiabatic susceptibility, $\chi'(H)/\chi'(0)$, were performed at 27 different temperatures between 4.5 and 16 K. The maximum field chosen at each temperature was kept so low that the field dependence of C_M estimated using Eq. (46) was always $< 0.2\%$. Under these conditions $r(H, T) \simeq r(T)$ and could be determined to an accuracy of about $\pm 0.2\%$ at the highest temperatures, increasing to about $\pm 1\%$ for the lowest temperatures. The zero-field specific heat, $C_M(0, T)$ was found using Eq. (44), estimating the expansion parameters θ, B_2, and B_3 iteratively, as will be discussed in Sec. VII. The values finally adopted were $\theta = 4.51 \pm 0.10$ K [corrected to the shape of the high-frequency sample (Sec. IV A 2)], $B_2 = 2.0 \pm 0.2$ K^2, and $B_3 = 1.4 \pm 0.6$ K^3. The final results are shown in Fig. 3 with a plot of $C_M(0, T)T^2/R$ vs $1/T$. The error bars represent the combined uncertainties resulting from the values of λ, θ^∞, B_2, and B_3 which were used in the analysis, as well as experimental errors in estimating $r(T)$. As one can see, the data become increasingly more accurate for higher temperatures. The large increase in the errors for the lowest temperatures is primarily due to the uncertainty in our estimate of θ^∞ (see Sec. VI E) and the experimental determination of $r(T)$.

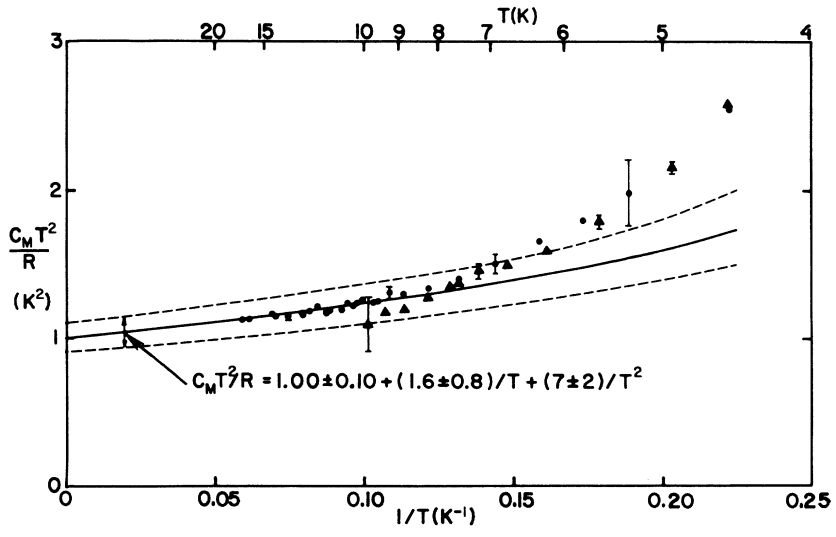

FIG. 3. High-temperature magnetic specific heat for $Tb(OH)_3$ as determined from high-frequency susceptibility measurements (filled circles) and calorimetric measurements (triangles). The results are plotted as $C_M T^2/R$ vs $1/T$ to identify the first three terms in the high-temperature expansion $C_M T^2/R = C_2 + C_3/T + C_4/T^2$. The solid line and broken lines indicate the high-temperature fit with error limits for $C_2 = 1.00 \pm 0.10$ K^2, $C_3 = 1.6 \pm 0.8$ K^3, and $C_4 = 7 \pm 2$ K^4. These were found from the high-temperature asymptotic behavior of the self-consistent fitting procedure described in the text.

Figure 3 also includes the calorimetric estimates of C_M, and it can be seen that they provide an excellent complement to the high-frequency measurements. The relatively close agreement between the two methods at the lowest temperatures ($T < 7$ K) is in fact very sensitive to the adequacy of the correction terms used in Eq. (44), since θ, B_2, and B_3 enter into the specific-heat analysis to the third power, whereas they only enter linearly into the more usual analysis of susceptibility measurements.[57] At higher temperatures, the correction terms become less important and we may therefore rely on the high-frequency measurements with even better confidence.

To estimate values of the leading high-temperature expansion coefficients [Eq. (16)] we fitted the combined high-frequency results between 4.5 and 16 K and the calorimetric data between 4.5 and 10 K iteratively to an expression of the form

$$C_M T^2/R = C_2 + C_3/T + C_4/T^2, \tag{50}$$

truncating the series arbitrarily at the third term, but using several choices of the number of experimental points to eliminate the effect from higher-order terms. This is discussed in detail in Sec. VII A. The results of this analysis gave a limiting set of values

$$\begin{aligned} C_2 &= 1.00 \pm 0.10 \text{ K}^2, \\ C_3 &= 1.60 \pm 0.8 \text{ K}^3, \\ C_4 &= 7 \pm 2 \text{ K}^4, \end{aligned} \tag{51}$$

where the increasing error limits on the higher-order terms reflect the uncertainty due to unknown higher-order terms.

The curve representing Eq. (50) in Fig. 3 clearly shows the asymptotic behavior of the fit at high temperatures. The increased discrepancy towards the lowest temperatures is readily explained by omission of higher-order terms in the expansion and can be removed by empirically adding one extra term

$$C_5 = 60 \pm 40 \text{ K}^5. \tag{52}$$

This value cannot be regarded as significant, but it does provide an estimate of the higher-order terms at temperatures where it is customary to assume only a significant $1/T^2$ specific heat.

The parameters C_2, C_3, and C_4 combined with an experimental value for θ^{∞} are sufficient to allow an unambiguous determination of the nondipolar interaction, as will be discussed in Sec. VII.

D. Entropy and Internal Energy of the Magnetic System

The internal energy $U_M(T)/R$ and entropy $S_M(T)/R$ are important thermodynamic quantities which will serve as useful checks on the analysis and the measurements. These could be determined directly from the magnetic specific heat, using the relationships

$$S_M(T)/R = \int_0^T (C_M^{\text{int}}/RT)\, dT \ , \tag{53}$$

$$U_M(T)/R = -\int_T^{\infty} (C_M^{\text{int}}/R)\, dT \ , \tag{54}$$

where the scales have been chosen so that $S_M(T)/R = 0$ for $T = 0$ K and $U_M(T)/R = 0$ for $T = \infty$. C_M^{int} represents the purely magnetic part related to the ionic interactions, obtained by subtracting from C_M the contributions from the crystal-field and hyperfine interactions (Sec. III C).

We will eventually want to consider $S_M(\infty)/R$ and $U_M(0)/R$, and integrations of C_M/R over all temperatures are therefore needed.[62] These are conveniently divided into three major sections. (a) $T \sim T_C$; the major contribution to the integrals comes from the range $T = 1.3$–5 K, where C_M is accurately known from the calorimetric measurements, as shown in Fig. 2. (b) $T \gg T_C$; for $T > 5$ K the asymptotic series given by Eqs. (16), (51), and (52) represents C_M adequately and the integrations to infinity could be performed analytically.[62] (c) $T \ll T_C$; similarly, for $T < 1.3$ K the asymptotic form given by Eqs. (37) and (49) can be integrated analytically to give the extrapolations to $T = 0$ K. Combining these contributions we finally estimate

$$S_M(\infty)/R = 0.68 \pm 0.06 \ , \tag{55}$$

in excellent agreement with the value $\ln 2 = 0.693$ expected for a system with effective spin $S' = \frac{1}{2}$, and

$$U_M(0)/R = -2.3 \pm 0.2 \text{ K} \ , \tag{56}$$

which is also in good agreement with other estimates, as will be discussed in Sec. VI G.

E. High-Temperature Zero-Field Susceptibility

The isothermal zero-field susceptibility was measured by two methods as described in Sec. V B. Both sets of data were corrected for shape to correspond to an infinite needle according to Eq. (5b) of I and the results are shown in Fig. 4, in which $(\chi_T T)^{-1}$ is plotted as a function of $1/T$. One can see that the results do not fall on a straight line as would be the case if a simple Curie-Weiss law described the data.

To find the best value of θ in Eq. (26) we followed an iterative procedure similar to that previously used in Ref. 1. An approximate value of $B_2 = 2.2 \pm 0.3$ K^2 was estimated from the low-temperature curvature in Fig. 4, and a modified susceptibility function defined to first order by $(\tilde{\chi}_T T)^{-1} = (\chi_T T)^{-1} - B_2/\lambda T^2$ was plotted as a function of $1/T$. This gave a much straighter curve from which a better high-temperature asymptote could be estimated.

To improve the analysis one step further we may note a special relation for the case of an Ising system between the susceptibility parameter B_2 and

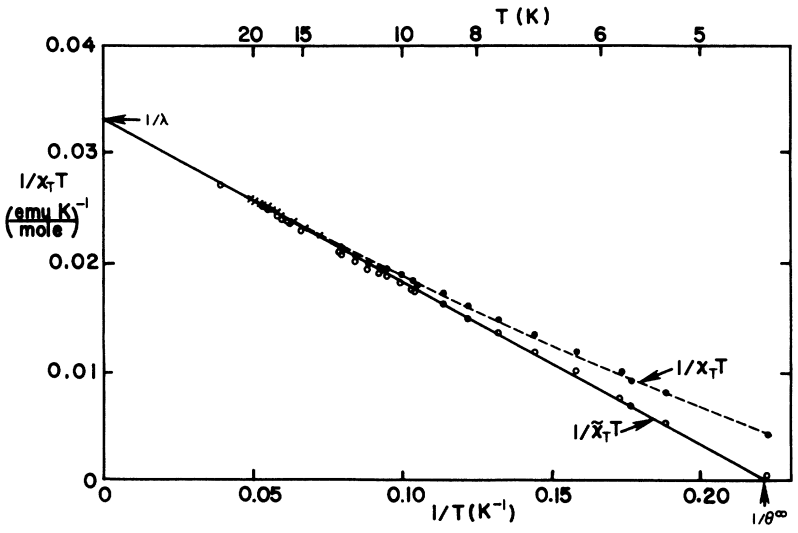

FIG. 4. High-temperature susceptibility of Tb $Tb(OH)_3$, corrected for shape to an infinite needle. The solid circles show the high-frequency results and the crosses the low-frequency results plotted as $1/\chi_T T$ vs $1/T$. To estimate the high-temperature asymptote, the results are also plotted (open circles) as $1/\tilde{\chi}_T T = 1/\chi_T T - (1/\lambda)(B_2/T^2 + B_3/T^3)$ vs $1/T$ with $B_2 = 2.0\ K^2$, $B_3 = 1.4\ K^3$, and $\lambda = 29.9$ emu K/mole (see text). The fitted full line corresponds to $1/\tilde{\chi}_T T = (1 - \theta^\infty/T)/\lambda$ with $\theta^\infty = 4.51 \pm 0.10$ K and $\lambda = 30.1 \pm 0.3$ emu K/mole.

the leading term of the specific-heat expansion C_2 [Eq. (30)]. Using the final value of $C_2 = 1.00 \pm 0.10\ K^2$ estimated in Sec. VI A we can therefore obtain a better estimate[62a] for $B_2 = 2.0 \pm 0.2\ K^2$. Furthermore, using Eq. (35) and the final iterated set of interaction parameters (Sec. VII), we can obtain an estimate for B_3: $B_3 = 1.4 \pm 0.6\ K^3$ and we are thus able to calculate an improved susceptibility function

$$\frac{1}{\tilde{\chi}_T T} = \frac{1}{\chi_T T} - \frac{1}{\lambda}\left(\frac{B_2}{T^2} + \frac{B_3}{T^3}\right), \tag{57}$$

which should be a much better approximation to $(1 - \theta^\infty/T)/\lambda$. The results are shown as the open circles in Fig. 4. It can be seen that a high-temperature asymptote can now be drawn with little uncertainty and we finally estimate

$$\lambda = 30.1 \pm 0.3 \text{ emu K/mole}$$

and

$$\theta^\infty = 4.51 \pm 0.10 \text{ K}.$$

The small curvature for $1/T > 0.15\ K^{-1}$ is presumably due to the higher-order terms in the series but these should have little effect in the range $0.05 > 1/T > 0.07\ K^{-1}$ used to estimate the asymptote. The error limits given above reflect our estimate of the corresponding uncertainty together with the errors in B_2 and the absolute calibration. The consistency of these results with other experiments will be discussed in Sec. VI H.

Low-frequency susceptibility measurements were also made below the ordering temperature and a number of striking nonlinear and irreversible effects were found. These effects are believed to be due to domain motion processes and they have been discussed elsewhere.[63]

F. Low-Temperature High-Field Magnetization

The magnetization as a function of applied field parallel and perpendicular to the crystal c axis for four temperatures between 1.1 and 4.2 K is shown in Fig. 5. The most striking features of these results are the rapid initial rise and large saturation magnetization for $M_{\parallel}$, and the much smaller, almost temperature-independent, linear variation of $M_{\perp}$.

The high-field saturation of $M_{\parallel}$ was analyzed to obtain a value for M_0 as outlined in Sec. IV D [Eq. (41)]:

$$M_0 = (4.95 \pm 0.04) \times 10^4 \text{ emu/mole},$$

which can also be expressed as $(9.0 \pm 0.1)\mu_B$/Tb ion. Using the value $V_0 = 36.7 \pm 0.4\ cm^3$ for the g atomic volume this can also be written

$$M_0 = 1349 \pm 20 \text{ emu/cm}^3,$$

which may be compared with the saturation magnetization of more common ferromagnets such as nickel and iron:

$$M_0(\text{Ni}) = 485 \text{ emu/cm}^3$$

and

$$M_0(\text{Fe}) = 1707 \text{ emu/cm}^3.$$

In marked contrast, the magnetization perpendicular to the c axis was more than 50 times smaller, even the highest fields, and consistent with an identically zero temperature-dependent contribution, as predicted by crystal-field theory (Sec. III C 2). The entire observed $M_{\perp}$ is therefore consistent with a second-order Van Vleck paramagnetism, and fitting all the data we estimate

$$\chi_{VV}^{\perp} = (6.8 \pm 1.1) \times 10^{-2} \text{ emu/mole},$$

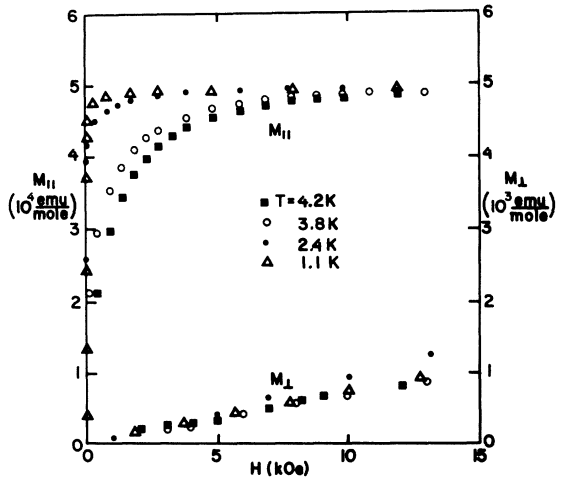

FIG. 5. High-field magnetization of $Tb(OH)_3$ parallel and perpendicular to the c axis at four temperatures between 1.1 and 4.2 K. Note the expanded scale for $M_\perp$ on the right-hand ordinate. The high-field values for $M_\parallel$ correspond to a saturation magnetization $M_0 = (4.95 \pm 0.04) \times 10^4$ emu/mole which is equivalent to $(9.0 \pm 0.1)\mu_B$/ion. The results for $M_\perp$ correspond to a field- and temperature-independent susceptibility $\chi_{VV}^{\perp} = (6.8 \pm 1.1) \times 10^{-2}$ emu/mole, which is consistent with the calculated Van Vleck paramagnetism.

in reasonable agreement with the calculated value $\chi_{VV}^{\perp} = 5.9 \times 10^{-2}$ emu/mole (Sec. III C 2).

These results are therefore also consistent with a value $g_\perp \equiv 0$, which we expect from the crystal-field analysis (Sec. III A), and a simple calculation shows that one must have $g_\perp < 1$ to stay within the error limits indicated above. This relatively large uncertainty on $g_\perp$ should not really be interpreted as indicating that $g_\perp$ might in fact be finite, but more of a measure of the difficulty of estimating a small transverse component in the presence of a much larger $g_\parallel$.

As would be expected, measurements of the paramagnetic moments ($M_\perp$ and $M_\parallel$) were completely reversible at the higher temperatures, but some hysteresis was found for $M_\parallel$ at the lowest temperatures. However, the effects were extremely small, rising to a maximum coercive field of 6 Oe at 1.1 K, and thus of no consequence to the present study.

G. Low-Field Magnetization near T_C

Additional low-field magnetization measurements were made to study the nature of the cooperative transition near 3.7 K. The results of these measurements are shown in Fig. 6, where we have plotted $M_\parallel$ as a function of the applied field.[64] At first it was hoped that these measurements would yield values of the critical exponents β and γ[65] as well as an estimate T_C, but as we shall see only qualitative information could be obtained with the samples available at this time.

The analysis was made following the work of Kouvel and Fisher,[66] and as a first step this involved plotting isotherms of $M_\parallel^2$ as a function of $H/M_\parallel$.[67,68] The results of such a plot are shown in Fig. 7. Extrapolating the isotherms to $H = 0$ we then find the initial susceptibility $\chi_T(0)$ and the results for this are shown in Fig. 8.

It can be seen that $\chi_T(0)$ tends to a constant value, characteristic of a ferromagnetic system whose susceptibility is limited by a demagnetizing field, and from the asymptotic value we can extract the effective demagnetizing factor for our particular sample. The value found was $N_\parallel = 0.099 \pm 0.010$ (in units for which a sphere is $\frac{4}{3}\pi$), and it can be seen that our sample was in fact quite a good approxi-

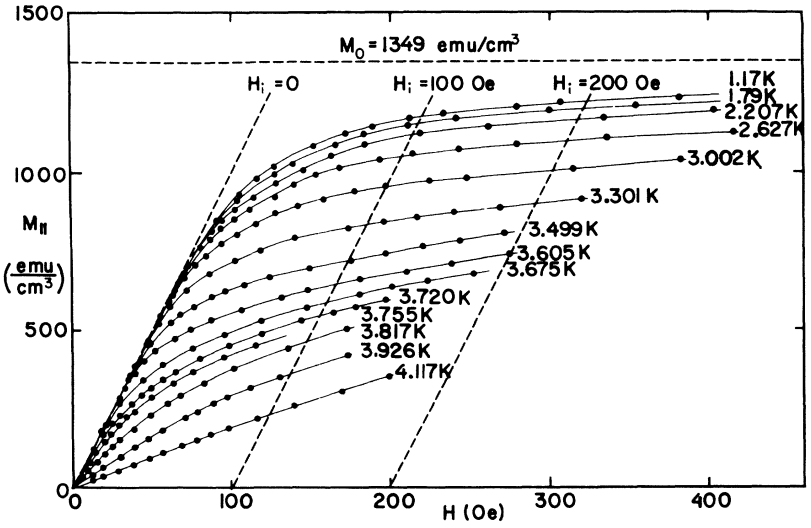

FIG. 6. Low-field variation of $M_\parallel$ for $Tb(OH)_3$ as a function of applied magnetic field, for several temperatures near T_C. Dashed lines of constant *internal* field are shown for $H_i = 0$, 100, and 200 Oe. The high-field saturation magnetization $M_0 = 1349$ emu/cm^3 is indicated by the horizontal broken line.

mation to an infinite needle. However, this was really not an advantage since it made the susceptibility more sensitive to other limiting factors such as inhomogeneities due to the nonellipsoidal sample shape. Evidence for some problem of this kind can be seen in Fig. 8, which shows a gradual transition ranging from about 3.60 to 3.75 K which is almost certainly not an intrinsic property of $Tb(OH)_3$.

Under these conditions it is clearly impossible to extract a precise value for T_C and to proceed with the kind of more detailed analysis outlined by Kouvel and Fisher.[66] However, we can estimate an approximate value for $T_C = 3.72 \pm 0.01$ K from the "knee" of the curve in Fig. 8, and this is in excellent agreement with the earlier estimate derived from the zero-field specific-heat measurements.

We may also note another interesting feature of the χ_T^{-1} curve in that it appears to approach a straight line only a short distance above T_C with a slope almost equal to that of the high-temperature Curie-law asymptote. One may speculate that this unusual behavior is related to the competition between the near-neighbor interactions and the consequent importance of the long-range dipolar interactions, and we shall discuss this question further in Sec. VII B. From a practical point of view it implies an extremely short temperature interval in which we might hope to study the *asymptotic* critical behavior, and it would seem that it will be very difficult to determine the critical exponent γ in this system. But before any such study can be undertaken, the cause of the apparently spurius rounding in the vicinity of T_C will have to be removed, and this presumably will have to await much larger samples which can be shaped into proper ellipsoids.

Evidence of the problems caused by the nonellipsoidal shape of the present samples can also be seen in the isotherms for $T < T_C$ in Fig. 7. Instead of starting at a finite value $M_s(T)$ at the ideal field for technical saturation ($H_s = N_{\parallel} M_{\parallel}$), and increasing slowly for higher fields, all the isotherms show a gradual variation which extends over a range of 10 to 100% of the ideal saturating field, and it is clearly impossible to estimate the true spontaneous magnetization. In absolute terms the effect is quite small, since $N_{\parallel}$ itself is so small, but it still vitiates completely any attempt to determine the critical exponent β. Even so, the general form of the results for $T < T_C$ leaves no doubt that $Tb(OH)_3$ orders ferromagnetically, and from the extreme anisotropy we can be sure that it must be a simple collinear state with all spins parallel to the c axis. This feature might ultimately prove to be very useful in resolving the complications due to the domain structure, and of course it greatly simplifies any theoretical discussion of the ordered state.

H. Summary of Characteristic Parameters

The parameters determined in Secs. VI B–G are summarized in Tables III and IV. For completeness we have also included a number of related parameters taken from the literature. There are a number of possible cross checks between the parameters which have already been discussed. λ and M_0 can be related to $g_{\parallel}$, using the expressions for λ and M_0 given in connection with Eqs. (26) and (41), and we see from Table III that the consistency between the three experimental determinations and the theoretical calculation is very good.

We can similarly relate Δ_0, U_0/R, and θ^{∞} using Eqs. (38) and (40), and comparing the values given

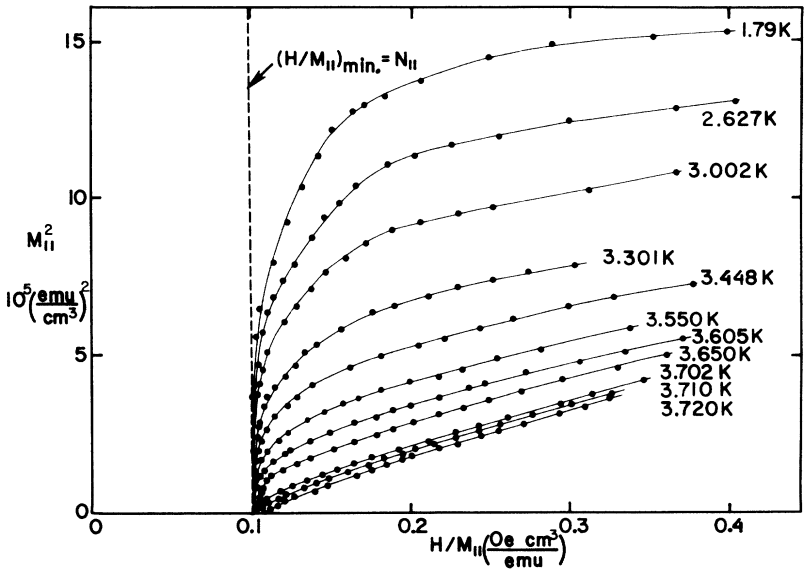

FIG. 7. Variation of $M_{\parallel}^2$ as a function of $H/M_{\parallel}$ for $Tb(OH)_3$ in the vicinity of T_C. For $T < 3.72$ K, $H/M_{\parallel}$ reaches a minimum value 0.099 ± 0.010 which we interpret as the effective demagnetizing factor $N_{\parallel}$ for our particular sample.

TABLE III. Single-ion and crystallographic parameters for $Tb(OH)_3$.

Parameter	Value	Method of Determination
$g_{\parallel}$	18.0 ± 0.2	Saturation magnetization[a]
	17.9 ± 0.2	Curie constant[a]
	17.7 ± 0.2	Optical absorption[b]
	17.87 ± 0.05	Crystal-field calculation[b]
$g_{\perp}$	0	Crystal-field calculation[b]
	<1	Low-T, high-H magnetization[a]
λ (emu K/mole)	30.1 ± 0.3	High-T susceptibility[a]
M_0 (emu/mole)	$(4.95 \pm 0.04) \times 10^4$	Low-T, high-H magnetization[a]
χ^{+}_{VV} (emu/mole)	$(6.8 \pm 1.1) \times 10^{-2}$	Low-T, high-H magnetization[a]
a (Å)	6.28 ± 0.01	X-ray diffraction[c]
c (Å)	3.57 ± 0.01	
V_0 (cm^3)	36.7 ± 0.4	Calculated from x-ray structure
b_{hyp} (K^2)	0.029 ± 0.001	Calculated from EPR results[d]
	0.032 ± 0.003	Low-T, zero-field specific heat[a]
Θ_D (K)	183 ± 3	Estimated from high-T specific heat[a,e]
ϵ_0 (K)	0.4 ± 0.1	Crystal-field calculations[f]
E_1 (K)	170.0 ± 0.2	Optical absorption[g]

[a] This work.
[b] Reference 4.
[c] Reference 11.
[d] Equation (11).
[e] Θ_D is defined in terms of only the Tb^{3+} ions, using $C_L/R = 234(T/\Theta_D)^3$.
[f] Reference 14.
[g] Reference 4.

in Table IV we see that the consistency is again very good. Taking a weighted mean of the different results we can estimate the "best" experimental value which will be used in Sec. VII A for the determination of the nondipolar spin-spin interactions. These values are given in Table V, together with the corresponding best estimates of C_2, C_3, and C_4, and the best value for $g_{\parallel}$ which was used to calculate the dipolar interactions.

VII. EFFECTIVE SPIN-SPIN INTERACTIONS IN $Tb(OH)_3$

A. Determination of Nondipolar Interactions

The four parameters θ^{∞}, C_2, C_3 and C_4 listed in Table V are more than sufficient to determine the three unknown parameters K_1, K_2, and K_3 with which we have characterized the nondipolar interactions. As discussed in Sec. III B, we would really expect significant nondipolar interactions only between nearest and next-nearest neighbors (characterized by K_1 and K_2), but we include K_3 in our analysis to allow for the possibility of a small but finite interaction between third-nearest neighbors. The results will show that K_3 is in fact extremely small, and we shall infer from this that other more distant neighbors will interact even more weakly.

An argument of this kind must be used with care since it might be possible for the contributions of several more distant neighbors to cancel, but we can fortunately rule this out in the present case on both theoretical and experimental evidence. The theoretical argument simply recognizes the fact that all of the most likely nondipolar interaction mechanisms fall off monotonically at large distances and any oscillatory behavior such as is found in metals is thus very unlikely. The experimental evidence is also only qualitative but it would seem quite unlikely that several more-distant-neighbor interactions could contribute to C_2 which is a sum of *squares* of the individual interactions, without exceeding the rather small observed value. We can therefore be fairly confident in the present case that the three parameters K_1, K_2, and K_3 are sufficient to describe the nondipolar interactions.

To determine the corresponding values we can fit Eqs. (23)–(25) and (32) to the experimental results, but this cannot be done in a straightforward way since the analysis of the experiments themselves requires knowledge of some of the higher-order expansion coefficients. These must first be estimated either empirically or theoretically and to accomplish this, we used an iterative computer procedure.

The basic input parameters for the analysis were θ^{∞}, C_2, C_3, and C_4, and in the first iteration approximate values of these were obtained from the experimental data by assuming the higher-order terms B_2, B_3, C_5, C_6, etc., to be negligible. Sub-

TABLE IV. Collective parameters for $Tb(OH)_3$ determined from asymptotically exact theory.

Parameter	Value	Method of determination
Δ_0 (K)	8.5 ± 0.5	Low-T, zero-field specific heat[a]
	9.2 ± 0.3	Optical absorption[b]
$-U_0/R$ (K)	2.3 ± 0.2	Integrated specific heat[a]
θ^{∞} (K)	4.51 ± 0.10	High-T, high- and low-frequency susceptibility[a,c]
B_2 (K^2)	2.2 ± 0.3	High-T, high-frequency susceptibility[a]
	2.0 ± 0.2[d]	High-T, high-frequency specific heat[a,e]
B_3 (K^3)	1.4 ± 0.6	Reference f
C_2 (K^2)	1.00 ± 0.10[g]	Fitted to high-T C_M measurements[a]
C_3 (K^3)	1.6 ± 0.8	Fitted to high-T C_M measurements[a]
C_4 (K^4)	7 ± 2	Fitted to high-T C_M measurements[a]

[a] This work.
[b] Reference 5.
[c] Analysis of $1/\tilde{\chi}_T T$ using iteratively estimated values of B_2 and B_3 (Sec. VII A).
[d] See *note added in proof* (Ref. 62a).
[e] Using Eq. (30).
[f] Calculated fron Eq. (35) using iteratively fitted K's.
[g] Includes a small contribution 0.07 K^2 from the hyperfine interaction [Eq. (11)] and the ground-state splitting [Eq. (14)].

TABLE V. Final set of characteristic parameters used for analysis of the interactions.

Parameter	Value	Method of Determination
θ^∞ (K)	4.51 ± 0.10	Weighted mean of the values found from θ^∞, Δ_0, and U_0/R in Table IV[a]
C_2 (K^2)	1.00 ± 0.10[b]	High-T C_M measurements
C_3 (K^3)	1.6 ± 0.8	High-T C_M measurements
C_4 (K^4)	7 ± 2	High-T C_M measurements
$g_{\|\|}$	17.87 ± 0.05	Weighted mean of crystal-field calculation and values found from M_0, λ, and optical spectra.[c]

[a] Using Eqs. (38) and (40).

[b] Includes a small contribution 0.07 K^2 from the hyperfine interaction [Eq. (11)] and the ground-state splitting [Eq. (14)].

[c] Using the expressions given in relation to Eqs. (26) and (41).

stituting these results into Eqs. (23)–(25) and (34) yielded first-order approximations for K_1, K_2, and K_3, and these could then be used in Eqs. (30) and (35) to estimate values for B_2 and B_3. Using these with Eq. (57) in the analysis of $1/\chi T$ next gave an improved value for θ^∞, as described in Sec. VI E, and substituting this together with the previous estimates of B_2 and B_3 into Eq. (44) resulted in a more accurate determination of the high-frequency specific heat for the start of the next and more difficult part of the iteration procedure.

This involved the determination of the parameters C_2, C_3, and C_4 from the measured C_M. To a first approximation these parameters could be estimated by fitting C_M to Eq. (50) and neglecting the higher-order terms C_5/T^5, C_6/T^6, etc., but for an accurate analysis the effect of these terms may be quite significant. Unfortunately, the calculation of the higher-order specific-heat parameters in terms of the K's is prohibitively difficult, and a simple iterative procedure similar to that used to estimate θ^∞ was therefore not possible. Instead, a strictly empirical approach was used, relying on the fact that the higher-order terms would affect the lower-temperature results more than the higher-temperature results. Thus by reanalyzing the data with successively fewer and fewer low-temperature points, one would expect to find results which would tend systematically to asymptotic values valid at high temperatures, and this was indeed found.

In the first fit, all of the data points between 4.5 and 16 K were included but, as we might expect, the over-all fit was poor and the standard deviations on the final K's were quite large. Successively omitting data points below 7, 8, 9, and 10 K improved the standard deviations significantly, while the fitted K's varied only slightly, with a clear trend towards a well-defined final set of values. Omitting even more of the data points increased the standard deviations again, but without changing the final K's significantly. We could thus conclude that the effect of the higher-order terms had been eliminated to a good approximation, so that the fitted values of C_2, C_3, and C_4 gave a true measure of the *asymptotic* behavior.

The values of C_2, C_3, C_4, and θ^∞ obtained in this way could now be used as starting values for the next iteration cycle until a consistent set of parameters was obtained. In practice, the convergence was very rapid, showing that the various correction terms could be estimated with adequate accuracy.

The whole fitting procedure described above is illustrated schematically in Fig. 9, and it was carried out in practice using the Yale IBM 377/155 computer. The final set of fitted values for the ex-

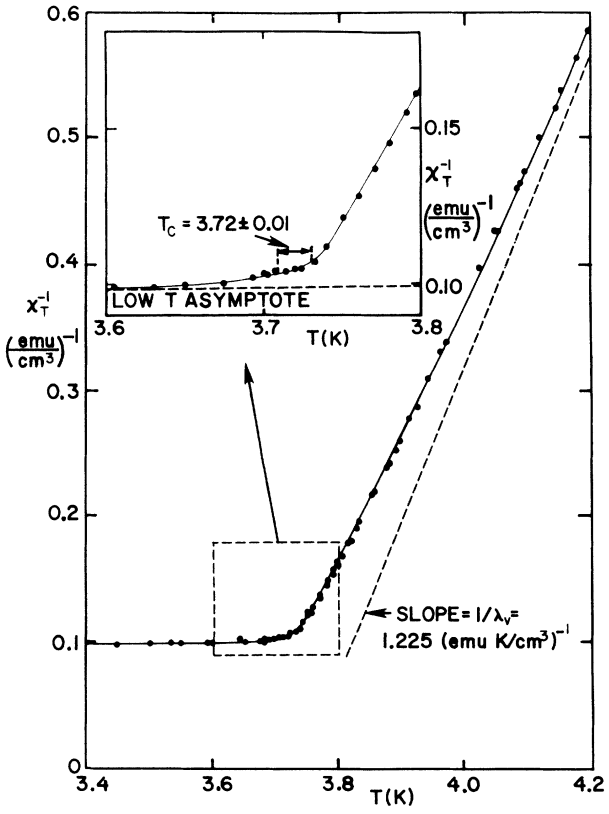

FIG. 8. Variation of $\chi_T^{-1}(0)$ as a function of temperature near T_C for $Tb(OH)_3$. The insert shows details of the curve very close to T_C, which is estimated to be 3.72 ± 0.01 K. The reason for the apparent rounding is not clear but it is probably due to the nonellipsoidal sample shape. The broken line represents the slope of the asymptotic high-temperature Curie-Weiss law $1/\lambda = 1.225$ (emu K/cm^3)$^{-1}$ for purposes of comparison. Note, however, that the actual Curie-Weiss line would come considerably further to the right since θ for this particular sample was about 4.43 K.

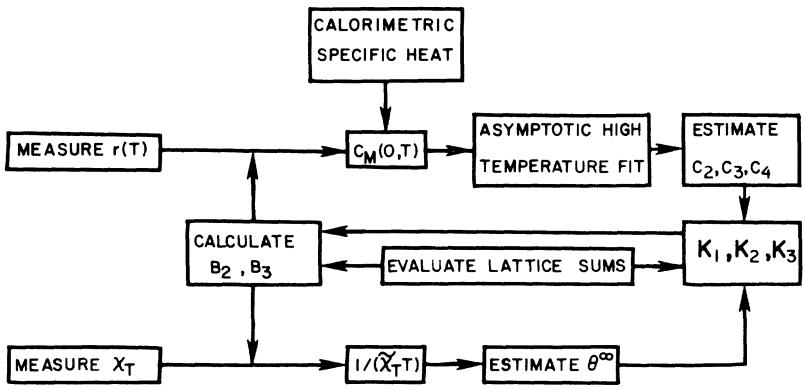

FIG. 9. Flow chart for determination of the nondipolar interaction constants as explained in text.

pansion coefficients is shown in Table V which includes estimated error limits to allow for uncertainties in the experiments and the lattice sum, as well as the effect of truncating the susceptibility and specific-heat series.

The corresponding final values of the nondipolar interactions were

$K_1 = 1.65 \pm 0.13$ K,

$K_2 = -0.43 \pm 0.10$ K,

$K_3 = 0.07 \pm 0.10$ K.

The error limits given here indicate the maximum ranges of values over which simultaneous solutions can be obtained consistent with the uncertainties in θ^∞, C_2, C_3, and C_4 given in Table V. The ranges are of course not independent, and the most probable values of the K's will fall well within these limits. We see therefore that the nondipolar interactions can be determined with very good accuracy, and we also see that K_3 is very small as we had suspected. These results are somewhat different from the preliminary values previously reported.[7] The reason for the difference may be found in the increased accuracy of the new measurements and also the fact that the more detailed analysis[8] has enabled us to choose between two sets of solutions which were previously indistinguishable.

The present solution also rules out large non-Ising interactions between any of the neighbors since these would contribute additional terms to C_2 which would all be necessarily positive, while the total must remain constant at the experimentally determined value. In fact, the non-Ising terms will almost certainly be very close to zero since the known crystal-field ground state allows only very-high-order off-diagonal terms, which are likely to be small, as discussed in Sec. III B.

It is quite instructive to examine a graphical solution of the K's as we did in the case of $Gd(OH)_3$.[1] This is shown in Fig. 10 where we have plotted the expressions for θ^∞, C_2, C_3, and C_4 given in Eqs. (23)–(25) and (34) as a function of K_1 and K_2, putting $K_3 = 0.07$ K and using the "experimental" values given in Table V. It can be seen that all four experimental bands overlap within a small range of K_1 and K_2, where point P indicates the final computer fit.

B. Comparison of Dipolar and Nondipolar Interactions

The fact that $Tb(OH)_3$ is an almost ideal Ising system is of course central to a discussion of the ordered state. The spins are strongly constrained to lie along the c axis and thus any sort of canted ordered spin arrangement is ruled out. An uncanted ferromagnetic ordered state is in fact also consistent with the direct measurements of the magnetization for $T < T_C$ (Sec. VI G), and with recent neutron diffraction experiments.[69] In the case of $Tb(OH)_3$ it is therefore natural to discuss the interactions in terms of the contributions to the interaction energy of a spin in this observed ferromagnetic ground state. In Table VI we list the different contributions for successive neighbors, and cumulative totals for successive shells of neighbors.

It can be seen that there are some remarkable near cancellations between several of the terms. In particular the strong nearest-neighbor magnetic dipole interaction D_1 is partly canceled by K_1, while the relatively weak D_2 is dominated by a somewhat stronger K_2 which is ferromagnetic in sign. If one looks at the contributions to the total energy from the different shells of neighbors it is apparent that no one shell is really dominant. Moreover, it is clear that the many far-neighbor magnetic dipole interactions will also combine to give a very significant total contribution to the energy of the ferromagnetic ground state. This contribution is largest for a long thin domain, and in that case it even exceeds the energy due to the near neighbors by a factor of more than 2. This suggests that the domains will be clusters of long chains parallel to the c axis.

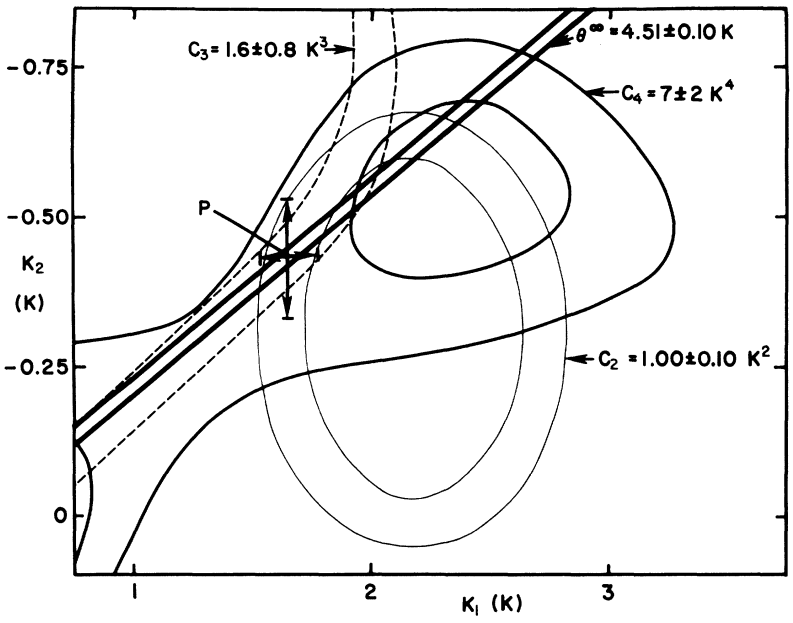

FIG. 10. Graphical solution for the nondipolar interaction constants K_1 and K_2 from the high-temperature series-expansion coefficients assuming $K_3 = 0.07$ K. (The curves would not change significantly if we would set $K_3 = 0$.) The bands in the figure include all of the solutions within the error limits of the expansion coefficients given in Table V as determined from Eq. (23) for $C_2 = 1.00 \pm 0.10\ K^2$; Eq. (24) for $C_3 = 1.6 \pm 0.8\ K^3$; Eq. (25) for $C_4 = 7 \pm 2\ K^2$; and Eq. (34) for $\theta^\infty = 4.51 \pm 0.10$ K. The region of simultaneous overlap corresponds to the computer solution $K_1 = 1.65 \pm 0.13$ K and $K_2 = -0.43 \pm 0.10$ K, as indicated by point P. The fact that the indicated error limits around P exceed the apparent region of overlap is due to the fixed value $K_3 = 0.07$ K for which this figure was drawn.

In view of the competition between the dipolar and nondipolar interactions for the nearest-neighbors, we might expect some unusual effects near the Curie point, where the effect of the long-range interactions will decrease. In particular, it might be possible for the system to develop quite complex short-range-order clusters reflecting the balance between the interactions, in contrast to a normal ferromagnet in which the correlations fall off monotonically with distance. The existence of oscillatory pair correlations has recently been established for some one- and two-dimensional Ising lattices with competing interactions.[70–72] If calculations could be extended to three-dimensional systems, $Tb(OH)_3$ would serve as a good test system which could readily be studied by neutron scattering techniques.

We are now also in a position to see why the susceptibility might show the unusual behavior which was found in the region just above T_C(see Fig. 8).

TABLE VI. Dipolar and nondipolar interactions in $Tb(OH)_3$.

Order of neighbor j	No. of neighbors n_j	Distance from origin r_{0j} (Å)	Dipole interaction energy per pair[a] D_j/k_B (K)	Nondipolar energy per pair[a] K_j/k_B (K)	Total contribution to energy of one spin from n_j neighbors $\frac{1}{2}n_j[(D_j+K_j)/k_B]$ (K)	Sum of contributions to energy per spin from all neighbors up to and including the jth shell $\sum \frac{1}{2}n_l[(D_l+K_l)/k_B]$ (K)
1	2	3.57	−2.187	1.65	−0.54	−0.54
2	6	4.04	0.313	−0.43	−0.35	−0.89
3	6	6.28	0.201	0.07	0.81	−0.08
4	6	6.47	−0.194		−0.58	−0.66
5	2	7.14	−0.273		−0.27	−0.93
...	...	...	...		...	...
11	12	9.76	0.0481		0.29	−0.65
					Total for all neighbors[b]	−2.26

[a]Signs relative to the observed ferromagnetic ground state. [b]Calculated for an infinitely long domain.

If the ferromagnetic ordering is really dominated by many small contributions from the more-distant neighbors, we would in fact expect mean-field-like behavior over a wider temperature range than usual, with deviations only very close to T_C.

However, this simple idea must not be taken too literally since we must note that the slope of the χ_T^{-1}-T curve is not really the same as that of the high-temperature asymptote $[\chi_T^{-1} = (T - 4.51)/\lambda]$ which, moreover, is significantly further to the right than the broken line shown in Fig. 8. The apparent linear behavior of χ_T^{-1} in the range 3.8–4.2 K must not therefore be taken to imply that the high-temperature asymptote has already been reached and it may in fact just be a complicated artifact of the various competing interactions. Clearly, some further theoretical work is called for, and we may hope that the detailed information which we have been able to extract about the interactions in this particular material will act as a spur for a renewed study of systems with both long- and short-range interactions.

VIII. SUMMARY AND CONCLUSIONS

The principal conclusion of this paper is that $Tb(OH)_3$ is an unusual example of a ferromagnetic Ising model. The Curie temperature is 3.72 K and the spin alignment is along the c axis of the hexagonal crystal structure.

The anisotropic *form* of the effective spin-spin interactions was established by a theoretical analysis based on previously established crystal-field eigenstates of the individual Tb^{3+} ions. Estimates of possible non-Ising showed that these should all be extremely small and this conclusion was supported by the final analysis of the experimental results.

The *magnitudes* of the individual spin-spin interactions were determined from an analysis of magnetic and thermal measurements in regions of temperature and field where asymptotically exact series expansions could be applied. From an examination of the crystal structure it seemed reasonable at the outset to assume that nondipolar interactions (exchange, electric multipole, etc.) should be much larger for the first- and second-nearest neighbors than the more distant neighbors, and this conclusion was confirmed by the final analysis. Values of the nondipolar interactions for the first, second, and third neighbors, K_n, are summarized in Table VI (column 5), and it can be seen that K_3 is in fact about 20 times smaller than K_1. (The error limits allow a range of 10 to ∞ for the ratio K_1/K_3.)

As usual, there is no explanation for either the sizes or signs of the nondipolar interaction parameters, which stand as a well-defined challenge to first-principles calculations of different interaction mechanisms.

The total spin-spin interactions may be found by adding the corresponding contributions of magnetic dipole-dipole coupling D_n calculated from the experimental g value and crystal structure. The results are given in Table VI (column 6) and it can be seen that there are remarkable cancellations between the two contributions for both the nearest and next-nearest neighbors. As a result, no one type of neighbor really dominates the cooperative properties and several of the near-neighbor interactions become comparable with the cumulative effects of the more-distant-neighbor interactions.

Thus, while $Tb(OH)_3$ is an almost ideal Ising system from the point of view of the $S_{zi} S_{zj}$ *form* of the interactions, it is quite different from the usual Ising models in the *range dependence* of its individual pair interactions. If the present theoretical calculations could be extended to simulate the effect of competition between several types of interactions, $Tb(OH)_3$ would serve as a most attractive test system.

ACKNOWLEDGMENTS

We would like to thank S. Mroczkowski and J. Eckert for growing the crystals used in these experiments and C. Sneider for his skillful building and maintenance of the apparatus described in this work.

---

†Work supported in part by the U.S. Atomic Energy Commission and in part by the National Science Foundation.

*Present address: RCA Laboratories, Princeton, N.J. 08540.

‡Present address: Corning Glass Works, Corning, N.Y. 14830.

[1]A. T. Skjeltorp, C. A. Catanese, H. E. Meissner, and W. P. Wolf, Phys. Rev. B 7, 2062 (1973), Paper I in the present series.

[2]We prefer to use the word nondipolar to the more usual exchange to emphasize the fact that there may also be contributions from electric-multipole and virtual-phonon interactions.

[3]W. P. Wolf, H. E. Meissner, and C. A. Catanese, J. Appl. Phys. **39**, 1134 (1968).

[4]P. D. Scott, H. E. Meissner, and H. M. Crosswhite, Phys. Lett. A **28**, 489 (1969).

[5]P. D. Scott and W. P. Wolf, J. Appl. Phys. **40**, 1031 (1969).

[6]H. E. Meissner and W. P. Wolf, J. Appl. Phys. **40**, 1038 (1969).

[7]A. T. Skjeltorp and W. P. Wolf, J. Appl. Phys. **42**, 1487 (1971).

[8]The analysis in the present paper is more complete than previously reported (Ref. 7) in that the number of terms in the high-temperature expansions of the specific heat, susceptibility, and magnetization have been extended from two to three, and the lattice sums have been recalculated.

[9]W. P. Wolf, J. Phys. (Paris) 32, C1-26 (1971).

[10]Other compounds with Tb^{3+} reported as good Ising-like systems include $TbAlO_3$ [L. Holmes, R. Sherwood, and L. G. Van Uitert, J. Appl. Phys. **39**, 1373 (1968)], and $Tb(C_2H_5SO_4)_3 \cdot 9H_2O$ [J. M. Baker and B. Bleaney, Proc. R.

Soc. A **245**, 156 (1958)], and $TbLiF_4$ [L. M. Holmes, T. Johansson, and H. J. Guggenheim, Solid State Commun. 12, 993 (1973)].

[11]P. V. Klevtsov and L. P. Sheina, Neorg. Materialy **1**, 912 (1965).

[12]For a discussion of the uncertainty in the lattice parameters see I, footnote 31.

[13]S. Mroczkowski, J. Eckert, H. Meissner, and J. C. Doran, J. Cryst. Growth **7**, 333 (1970).

[14]This splitting could not be resolved spectroscopically, and was only inferred from a full crystal-field analysis. See Ref. 4.

[15]We shall follow the usual custom of expressing all energy parameters in units of K, omitting the division by k_B, Boltzmann's constant.

[16]M. H. L. Pryce, Proc. R. Soc. A **63**, 25 (1950).

[17]P. M. Levy, Phys. Rev. **177**, 509 (1969).

[18]D. Smith and J. H. M. Thornley, Proc. Phys. Soc. Lond. **89**, 779 (1966).

[19]P. M. Levy, Phys. Rev. Lett. **20**, 1366 (1968).

[20]This was shown to be the case for the equally magnetically concentrated $Gd(OH)_3$ in I.

[21]Some indication of the non-Ising terms could have been obtained from the value of the spin-spin relaxation time τ_{SS} (see Ref. 22), but there are unfortunately no experimental estimates of τ_{SS} for $Tb(OH)_3$. One would generally expect quite a long τ_{SS} due to a slowing down of mutual spin flips in such an anisotropic system, but high-frequency susceptibility measurements reported later in this paper (Sec. V A) indicate $\tau_{SS} \lesssim 10^{-8}$ sec. This is not inconsistent with the finite non-Ising terms estimated here, but it is too short to set a closer upper limit.

[22]W. P. Wolf, B. Schneider, D. P. Landau, and B. E. Keen, Phys. Rev. B **5**, 4472 (1972).

[23]For the high-frequency specific-heat measurements, the Schottky specific heat is not present.

[24]The Schottky specific heat corresponds to about 40% of the *electronic* specific heat at $T = 17$ K, but as the uncertainty in E_1 is only about ± 0.2 K (Ref. 4), the corresponding error in the specific-heat correction from this source is quite negligible.

[25]J. H. Van Vleck, *The Theory of Electric and Magnetic Susceptibilities* (Oxford U. P., London, 1932), Chap. IX, p. 232.

[26]No experimental value for the diamagnetic susceptibility χ_d of $Tb(OH)_3$ is available, but is expected to be of order 10^{-5} emu/mole which would be quite negligible.

[27]Using the same crystal-field eigenfunctions, one finds for the parallel case $\chi_{VV}^{\parallel} = 3.2 \times 10^{-5}$ emu/mole, which is about a factor of 10 less than the sensitivity in the magnetization measurements.

[28]J. M. Baker and B. Bleaney, Proc. R. Soc. A 245, 156 (1958).

[29]A. Abragam and M. H. L. Pryce, Proc. R. Soc. Lond. **205**, 135 (1951).

[30]It has been shown by Elliot and Stevens (see Ref. 31) that $A/g_{\parallel} = B/g_{\perp} =$ constant as long as the crystal-field states are spanned by a single J multiplet. This is a good approximation in the present case, as the ground-state wave function for Tb^{3+} in $Tb(OH)_3$ is almost completely $J = 6$ (see Ref. 4).

[31]R. J. Elliot and K. W. H. Stevens, Proc. R. Soc. A **218**, 553 (1953).

[32]A. Abragam and B. Bleaney, *Electron Paramagnetic Resonance of Transition Ions* (Clarendon, Oxford, England, 1970), p. 306.

[33]D. C. Mattis and W. P. Wolf, Phys. Rev. Lett. **16**, 899 (1966).

[34]B. Bleaney, Phys. Rev. **78**, 214 (1950).

[35]One can easily obtain the exact result for C_{hyp}/R by calculating the Schottky anomaly from the four hyperfine levels in zero field. Comparison with the approximate result in Eq. (11) shows agreement to within about 4% down to 0.7 K.

[36]The reason for the slightly higher value for the experimental b_{hyp} compared to the calculated value is not clear at this point. It may be due to additional specific heat which is due to impurities, or to an error in the analysis, such as a finite value for Q. The most probable reason is, however, a small systematic error due to experimental difficulties arising from residual He^3 gas in the sample chamber. More detailed measurements below 1 K are needed to resolve this.

[37]The form of the high-temperature expansion used here is in accordance with the notation used later (Sec. IV A 2).

[38]R. J. Elliott, P. Pfeurty, and C. Wood, Phys. Rev. Lett. **25**, 443 (1970).

[39]W. Opechowski, Physica (Utr.) **4**, 181 (1937).

[40]J. H. Van Vleck, J. Chem. Phys. **5**, 320 (1937).

[41]J. M. Daniels, Proc. Phys. Soc. Lond. **66**, 673 (1953).

[42]A description of the programs used may be obtained from the authors on request.

[43]C. D. Marquard, Proc. Phys. Soc. Lond. **92**, 650 (1967).

[44]We follow the notation used in I and Ref. 43. The particular form used is most convenient because the entire shape dependence of χ_T will appear in the first term of the expansion, whereas in an expansion of form $\chi_T(0) = (\lambda/T)(1 + \theta/T + B'_2/T^2 + \cdots)$ one has the shape dependence in all terms: θ, B'_2, B'_3, ...

[45]The moment due to the Van Vleck paramagnetism (Sec. III C 2) will be quite negligible and is not considered here.

[46]A quite detailed discussion of an analogous system, dysprosium aluminum garnet, has been given in Ref. 22.

[47]D. P. Landau, B. E. Keen, B. Schneider, and W. P. Wolf, Phys. Rev. B **3**, 2310 (1971).

[48]R. B. Clover and W. P. Wolf, Rev. Sci. Instrum. **41**, 617 (1970).

[49]A. T. Skjeltorp and W. P. Wolf, Phys. Rev. B **8**, 215 (1973).

[50]F. R. McKim and W. P. Wolf, J. Sci. Instrum. **34**, 64 (1957).

[51]H. B. G. Casimir and F. K. du Pré, Physica (Utr.) **5**, 507 (1938).

[52]C. J. Gorter, *Paramagnetic Relaxation* (Elsevier, New York, 1947).

[53]R. Orbach, Proc. Phys. Soc. Lond. A **264**, 468 (1961).

[54]A. T. Skjeltorp, thesis (Yale University, 1971) (unpublished).

[55]The simple energy-level structure of $Tb(OH)_3$ as determined spectroscopically (Ref. 4) excludes the possibility that the apparent kink in the C_M curve could be genuine effect arising from population of a low-lying electronic state or a crystallographic phase transition.

[56]W. J. Caspers, *Theory of Spin Relaxation* (Interscience, New York, 1964).

[57]A. T. Skjeltorp and W. P. Wolf, AIP Conf. Proc. **5**, 695 (1972).

[58]Normally this expression is a simplified version assuming $\chi_T(H)/\chi_T(0) = 1$ and $C_M(H, T) = C_M(0, T)$ field independent. See, for example, Ref. 48.

[59]By using relatively high fields, Eq. (46) for the field dependence of C_M could be verified within experimental error. This was also taken as an indication that no spin-spin relaxation was present.

[60]S. Foner, Rev. Sci. Instrum. **30**, 548 (1959).

[61]These figures refer to one particular pair of pickup coils which has a total of 80 000 turns of 46-AWG copper wire. In practice this was close to the limit which could be used with the ballistic galvanometer due to its critical damping resistance of 300 Ω, but, for the digital voltmeter, larger coils with thinner wire might have been used.

[62]As usual, integration "to infinity" here implies $T \gg T_C$, but $\ll E_1/k_B$.

[62a]*Note added in proof.* It has been pointed out to us by M. Teplov and B. Z. Malkin that this application of Eq. (30) is not quite corrected, since Eq. (30) only refers to those parts of B_2 and C_2 which depend on the Ising-like spin-spin interactions. Thus we should really write $B_2^{\text{int}} = 2C_2^{\text{int}} = 2[C_2 - (C_2)_{\text{hyp}} - (C_2)_{cf}]$ $= 1.86\ \text{K}^2$, and since the nuclear and crystal-field contributions to B_2 are negligible (see Sec. III C), this value provides a better estimate for B_2 than the value $2.0 \pm 0.2\ \text{K}^2$ given in the text. However, since B_2 is only used for small correction terms and the change is less than the quoted uncertainty, we shall not make the appropriate revisions in the rest of this paper.

[63]A. Schlachetzki and J. Eckert, Phys. Status Solidi **11**, 611 (1972).

[64]The magnetization results in this section will be expressed in units of emu/cm^3 in contrast to the units of emu/mole used previously. This is to simplify the discussion of demagnetizing effects which will here turn out to be very important.

[65]See, for example, M. E. Fisher, Rep. Prog. Phys. **30**, 615 (1967).

[66]J. S. Kouvel and M. E. Fisher, Phys. Rev. **136**, A1626 (1964).

[67]K. P. Belov and A. N. Goryaga, Fiz. Met. Metalloved. **2**, 3 (1956).

[68]J. S. Kouvel, General Electric Research Laboratory Report No. 57-RL-1799, 1957 (unpublished).

[69]V. Minkiewicz (private communication).

[70]J. Stephenson, Phys. Rev. B **1**, 4405 (1970).

[71]J. Stephenson, Can. J. Phys. **47**, 2621 (1969); Can. J. Phys. **48**, 1724 (1970).

[72]J. Stephenson, J. Math. & Phys. **11**, 413 (1970); J. Math. & Phys. **11**, 420 (1970).